

Fullerene complexes with divalent metal dithiocarbamates: structures, magnetic properties, and photoconductivity

D. V. Konarev,^{a*} S. S. Khasanov,^b D. V. Lopatin,^c V. V. Rodaev,^c and R. N. Lyubovskaya^a

^aInstitute of Problems of Chemical Physics, Russian Academy of Sciences,
1 prosp. Akad. Semenova, 142432 Chernogolovka, Moscow Region, Russian Federation.

Fax: +7 (496) 522 1852. E-mail: konarev@icp.ac.ru

^bInstitute of Solid State Physics,

2 ul. Institutskaya, 142432 Chernogolovka, Moscow Region, Russian Federation.

E-mail: khasanov@issp.ac.ru

^cG. R. Derzhavin Tambov State University,

33 ul. Internatsionalnaya, 392000 Tambov, Russian Federation.

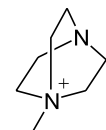
E-mail: lopatin@tsu.tmb.ru

A series of complexes of fullerenes C₆₀ and C₇₀ with metal dithiocarbamates {M^{II}(R₂dtc)₂}·C_m (m = 60 or 70) and metal dithiocarbamates coordinated to nitrogen-containing ligands (L), {M^{II}(R₂dtc)₂}_x·L·C₆₀ (x = 1 or 2), where M = Cu, Zn, Cd, Hg, Mn, or Fe, R = Me, Et, Prⁿ, Prⁱ, or Buⁿ, L is 1,4-diazabicyclo[2.2.2]octane (DABCO), *N,N'*-dimethylpiperazine, or hexamethylenetetramine, were synthesized. The shape of dithiocarbamate molecules is sterically compatible with the spherical shape of C₆₀, resulting in an efficient interaction between their π systems. The resulting compounds are characterized by a layered or three-dimensional packing of the fullerene molecules. In the C₆₀ complexes, iron(II) and manganese(II) dithiocarbamates exist in the high-spin states (S = 2 and 5/2). The magnetic susceptibility of {M^{II}(Et₂dtc)₂}·C_m (M = Fe or Mn, m = 60 or 70) in the temperature range of 200–300 K is described by the Curie–Weiss law with Θ = –250 and –96 K and with maxima at 110 and 46 K, respectively, which is indicative of a strong antiferromagnetic spin coupling between M^{II}. The Weiss constants for the [{M^{II}(Et₂dtc)₂}₂·DABCO]·C₆₀·(DABCO)₂ complexes (M = Fe or Mn) are 1.7 and 0.3 K, respectively. The magnetic moments of the complexes containing Fe and Mn dithiocarbamates slightly increase at temperatures below 50 and 35 K, respectively, which is evidence of the ferromagnetic spin coupling between M^{II} in {M^{II}(Et₂dtc)₂}·DABCO. Single crystals of the complexes exhibit low dark conductivity (10^{–10}–10^{–11} S cm^{–1}). The visible light irradiation of these crystals leads to an increase in the photocurrent by two–three orders of magnitude. The photogeneration of free charge carriers in the complexes occurs both due to the photoexcitation of metal dithiocarbamate (Cu^{II}(Et₂dtc)₂) and through the charge transfer from metal dithiocarbamate (M^{II}(Et₂dtc)₂, M = Zn or Cd) to C₆₀.

Key words: donor-acceptor complexes, fullerene C₆₀, metal dithiocarbamates, crystal structure, magnetic properties, photoconductivity.

Donor-acceptor complexes of fullerenes are extensively studied in connection with their interesting optical and magnetic properties.^{1–3} Fullerene complexes were synthesized with different classes of donor molecules, such as aromatic hydrocarbons,^{4–6} tetrathiafulvalenes,^{7–9} amines,^{10,11} metalloporphyrins,^{12–14} metallocenes,¹⁵ etc.^{1,8,15} Metal tetraphenyl- and octaethylporphyrinates form a wide family of compounds with fullerenes, which have both neutral and ionic ground states.^{12–15} These complexes can be modified by introducing nitrogen-containing ligands (L) or cations (D⁺) to give the multicomponent complexes {(prf)_x·L}·C₆₀ or

{(D⁺)·(prf)·(C₆₀[–])}, where prf is porphyrin.^{16–20} For example, the coordinated mono-, di-, and tetranuclear zinc tetraphenylporphyrinates form the molecular complexes (ZnTPP_x·L)·C₆₀ with C₆₀ (TPP is tetraphenylporphyrin; x = 1, 2, or 4).^{16,17,20} The use of the coordinating *N*-methyl diazabicyclo[2.2.2]octane cation (MDABCO⁺) made it possible to synthesize a series of the multicomponent ionic complexes {(MDABCO⁺)·(Co^{II}prf)·C₆₀[–]·(Solv)} (Solv is solvent). The reversible formation of the diamagnetic coordinated species [(MDABCO⁺)·Co^{II}OEP·C₆₀[–]],¹⁸

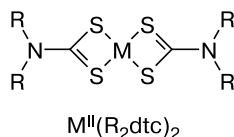


MDABCO⁺

where $\text{Co}^{\text{II}}\text{OEP}$ is cobalt(II) octaethylporphyrinate, and the formation of the unusual dimer $(\text{C}_{60}^-)_2$ linked by two C—C bonds are observed in these complexes.^{19,20}

These studies showed that the introduction of a nitrogen-containing ligand or cation into the complexes by the formation of additional coordination bonds between the nitrogen atom and the metal atom of the porphyrin ring allows the control of the structure of the resulting complexes and, in some cases, the charge state of fullerene and the physical properties of the complexes.

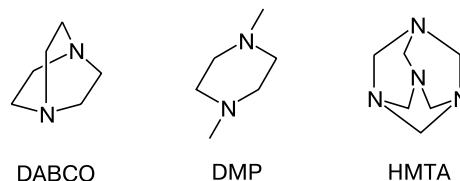
Metal dialkyldithiocarbamates $\text{M}^{\text{II}}(\text{R}_2\text{dtc})_2$ belong to a wide family of organometallic compounds having properties important for the design of donor-acceptor complexes with fullerenes.



Most of divalent metal dithiocarbamates adopt an open-book shape^{21–26} and are sterically compatible with the spherical shape of fullerene molecules. The structure of dithiocarbamates can be modified and their electron-donating properties can be varied with the use of various metals (M^{II}) and alkyl substituents of different length (R).²⁷ Some dithiocarbamates exhibit strong absorption in the visible light region ($\text{M} = \text{Cu}^{\text{II}}$ and Ni^{II}) or have unusual magnetic properties. For example, $\text{Fe}^{\text{III}}(\text{Et}_2\text{dtc})_2\text{Cl}$ is a one-component ferromagnet with $T_c = 2.46$ K.²⁸ Only a few metal dithiocarbamate complexes with π -acceptors, for example, tetracyanoquinodimethane complexes with molybdenum and tungsten dialkyldithiocarbamates,^{29,30} were characterized. We have synthesized^{31–33} a large series of complexes of fullerenes C_{60} and C_{70} with various metal dithiocarbamates ($\text{M} = \text{Cu}^{\text{II}}$, Cu^{I} , Ag^{I} , Zn , Cd , Hg^{II} , Mn^{II} , Ni^{II} , Pt^{II} , or Pd^{II}) and a large set of substituents (R = Me, Et, Prⁿ, Buⁿ, or CH_2Ph).

Metal dithiocarbamates, like metalloporphyrins, can form structures coordinated to nitrogen-containing ligands. Such compounds were prepared primarily with zinc and cadmium dithiocarbamates. These dithiocarbamates are linked together by bidentate ligands, such as 4,4'-bipyridine, bis(4-pyridyl)ethylene, or tetramethylethylenediamine, to form the dinuclear structures $\{\text{M}(\text{R}_2\text{dtc})_2\}_2 \cdot \text{L}$,^{34–36} whereas pyridine, imidazole, 2,2'-bipyridine, and phenanthroline give the mononuclear complexes $\{\text{M}(\text{R}_2\text{dtc})_2\} \cdot \text{L}$ with dithiocarbamates.^{37,38} It appeared that the cocrystallization of fullerene C_{60} with metal dithiocarbamates in the presence of diazabicyclooctane (DABCO), *N,N'*-dimethylpiperazine (DMP), or hexamethylenetetramine (HMTA) affords the C_{60} complexes with mono- or dinuclear metal dithiocarbamates coordinated to nitrogen-containing ligands,

$\{\text{M}^{\text{II}}(\text{R}_2\text{dtc})_2\}_x \cdot \text{L} \cdot \text{C}_{60}$ ($\text{M} = \text{Zn}$, Cd , Hg , Mn , or Fe ; R = Et, Pr^l, or Prⁿ; $x = 1$ or 2, L = DABCO, DMP, or HMTA).



In addition to the known complexes of zinc and cadmium dithiocarbamates, the formation of analogous structures of mercury(II), manganese(II), and iron(II) dithiocarbamates in fullerene complexes was observed for the first time.

In the present study, we synthesized the $\{\text{M}^{\text{II}}(\text{R}_2\text{dtc})_2\} \cdot \text{C}_{60}$, $\{\text{M}^{\text{II}}(\text{R}_2\text{dtc})_2\} \cdot \text{C}_{70}$, and $\{\text{M}^{\text{II}}(\text{R}_2\text{dtc})_2\}_x \cdot \text{L} \cdot \text{C}_{60}$ complexes ($x = 1$ or 2, L = DABCO, DMP, or HMTA), determined their crystal structures, and investigated the magnetic and photo-physical properties.

Results and Discussion

1. Synthesis of the complexes

The cocrystallization of dithiocarbamates with fullerenes can afford both the dinuclear complexes $\{\text{M}^{\text{II}}(\text{R}_2\text{dtc})_2\}_2$ and the mononuclear complexes $\text{M}^{\text{II}}(\text{R}_2\text{dtc})_2$. Dinuclear dithiocarbamates are formed as a result of the axial coordination of the sulfur atom to the metal atom of the adjacent dithiocarbamate molecule (Fig. 1). These compounds form the fullerene complexes $\{\text{Cu}(\text{EtMedtc})_2\}_2 \cdot \text{C}_{60}$ (**1**), $\{\text{M}^{\text{II}}(\text{R}_2\text{dtc})_2\}_2 \cdot \text{C}_{60}$ (**2–5**), where R = Et, M = Cu (**2**), Cd (**3**), Hg (**4**), or Fe (**5**), and $\{\text{Mn}(\text{Et}_2\text{dtc})_2\}_2 \cdot \text{C}_{70}$ (**6**). The dinuclear structures are known^{21–24} for copper(II), cadmium(II), and iron(II) dithiocarbamates. To our knowledge, these structures have been previously unknown for $\text{Hg}^{\text{II}}(\text{Et}_2\text{dtc})_2$ and $\text{Mn}^{\text{II}}(\text{Et}_2\text{dtc})_2$. The starting dithiocarbamate $\text{Hg}^{\text{II}}(\text{Et}_2\text{dtc})_2$ has a mononuclear planar structure;³⁹ $\text{Mn}^{\text{II}}(\text{Et}_2\text{dtc})_2$, a polynuclear structure.⁴⁰ In the complex with C_{60} , dithiocarbamate $\text{Zn}(\text{Et}_2\text{dtc})_2$ has a mononuclear tetragonal structure (see Fig. 1), although the starting compound has a dinuclear structure.^{25,26} Generally, crystals of C_{60} complexes with dithiocarbamates were grown by concentrating a solution containing fullerene and the corresponding metal dithiocarbamate. However, in the presence of cadmium(II), manganese(II), or iron(II) dithiocarbamates, the fullerene complexes $\{\text{M}^{\text{II}}(\text{Et}_2\text{dtc})_2\}_2 \cdot \text{C}_{60}$ and $\{\text{M}^{\text{II}}(\text{Et}_2\text{dtc})_2\}_2 \cdot \text{C}_{70}$ are almost completely precipitated as powders even from dilute solutions in C_6H_6 , PhCl, or $\text{C}_6\text{H}_4\text{Cl}_2$. Because of this, crystals of the complexes

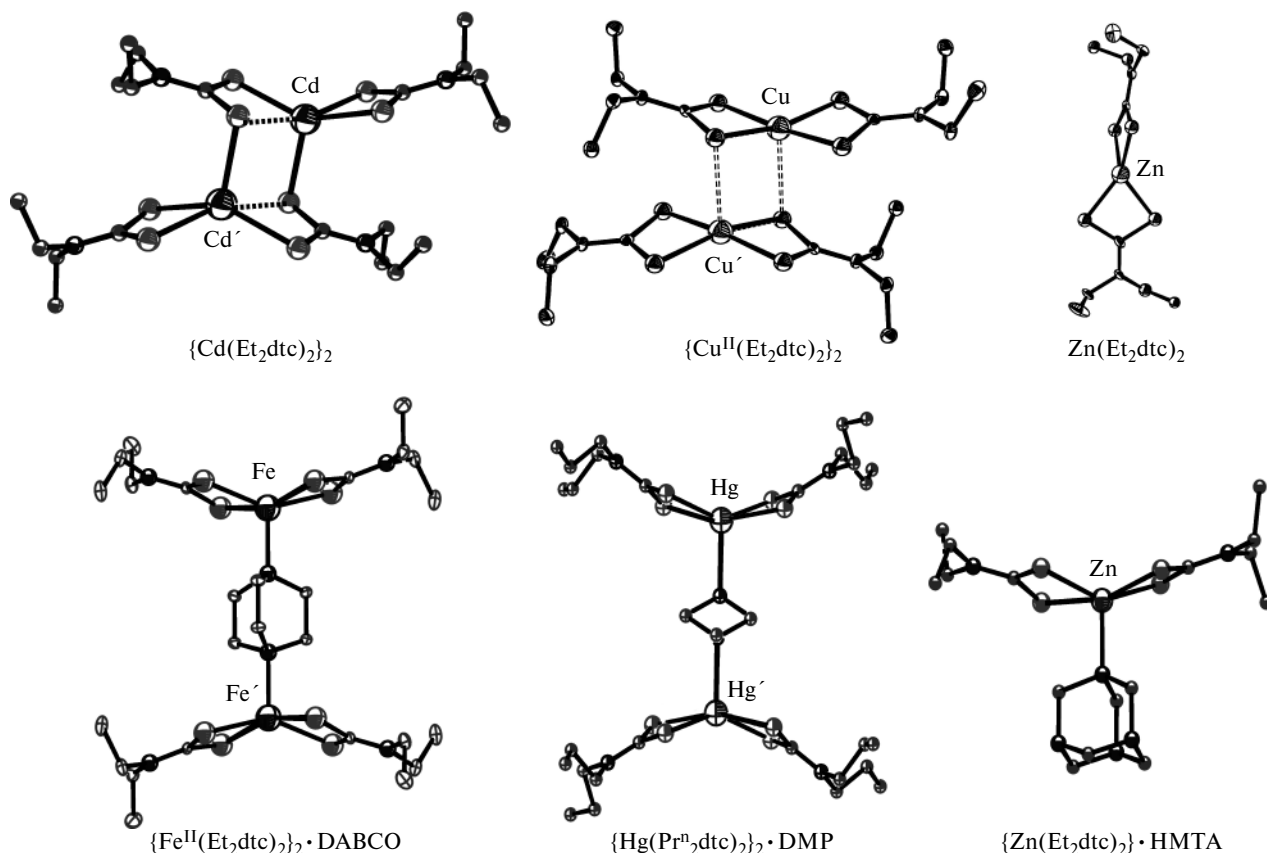
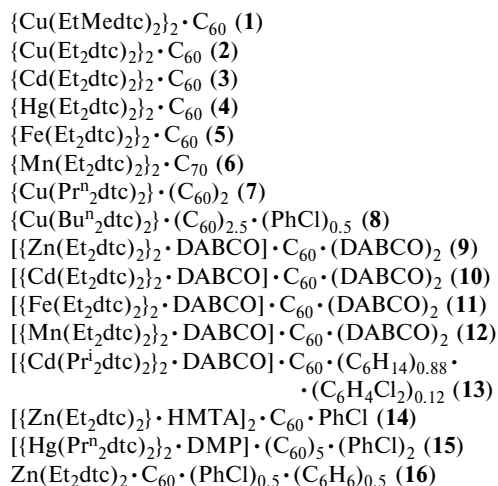


Fig. 1. Molecular structures of metal dithiocarbamates, both free and coordinated to nitrogen-containing ligands, in complexes with C_{60} : cadmium diethyldithiocarbamate, $\{Cd(Et_2dtc)_2\}_2$; copper(II) diethyldithiocarbamate, $\{Cu(Et_2dtc)_2\}_2$; zinc diethyldithiocarbamate, $Zn(Et_2dtc)_2$; iron(II) diethyldithiocarbamate coordinated to DABCO, $\{Fe(Et_2dtc)_2\}_2 \cdot DABCO$; mercury(II) di(*n*-propyl)dithiocarbamate coordinated to DMP, $\{Hg(Pr^n_2dtc)_2\}_2 \cdot DMP$; and zinc diethyldithiocarbamate coordinated to hexamethylenetetramine, $\{Zn(Et_2dtc)_2\} \cdot HMTA$.

with these dithiocarbamates were grown by the slow diffusion method.

The fullerene-rich complexes $\{Cu^{II}(R_2dtc)_2\} \cdot (C_{60})_m$ ($m = 2$ (7) or 2.5 (8)) are formed by Cu^{II} dithiocarbamates containing long alkyl substituents (Pr^n or Bu^n). Apparently, these complexes have a planar mononuclear structure. These structures are also characteristic of Ni^{II} and Pt^{II} dithiocarbamates, which form complexes with C_{60} of the analogous composition $\{M(Pr^n_2dtc)_2\} \cdot (C_{60})_2$.³²

It should be noted that metal dithiocarbamates $M^{II}(R_2dtc)_2$ ($M^{II} = Zn, Cd, Hg, Mn,$ and Fe) are prone to extra coordination, whereas the introduction of the third component, *viz.*, the coordinating ligand DABCO, DMP, or HMTA, into the synthesis results in the formation of fullerene complexes with mono- and dinuclear metal dithiocarbamates, in which the dithiocarbamates are coordinated to these ligands. The length of alkyl substituents in dithiocarbamates plays an important role. Complexes with DABCO (9–13) and HMTA (14) (see Fig. 1) can be synthesized only with dithiocarbamates containing the Et or Pr^i substituents.



Dithiocarbamate $Hg^{II}(Et_2dtc)_2$ does not coordinate DABCO; instead, the $\{Hg(Et_2dtc)_2\}_2 \cdot C_{60}$ complex (4) is crystallized. Complexes of C_{60} with dialkyldithiocarbamates coordinated to DMP, for example,

Table 1. Bond lengths in metal(II) dithiocarbamates, both free and coordinated to nitrogen-containing ligands

| Complex | Structural unit | Metal | R | Ligand | Bond length/Å | | | | |
|-----------|--|-------|-----------------|--------|---------------|------------|------------|------------|------------|
| | | | | | <i>a</i> | <i>b</i> | <i>c</i> | <i>d</i> | M—S* |
| 2 | [M ^{II} (R ₂ dtc) ₂] ₂ | Cu | Et | — | 2.3354(8) | 2.2978(8) | 2.2994(9) | 2.3218(8) | 3.030(1) |
| 3 | [M ^{II} (R ₂ dtc) ₂] ₂ | Cd | Et | — | 2.8771(10) | 2.544(9) | 2.5333(10) | 2.6330(10) | 2.5988(12) |
| 4 | [M ^{II} (R ₂ dtc) ₂] ₂ | Hg | Et | — | 3.1672(8) | 2.5046(7) | 2.6259(7) | 2.4629(7) | 2.6994(7) |
| 10 | [M ^{II} (R ₂ dtc) ₂] ₂ ·L | Cd | Et | DABCO | 2.7050(2) | 2.5438(2) | 2.5438(2) | 2.7050(2) | — |
| 11 | [M ^{II} (R ₂ dtc) ₂] ₂ ·L | Mn | Et | DABCO | 2.4872(4) | 2.5971(5) | 2.5971(5) | 2.4872(4) | — |
| 12 | [M ^{II} (R ₂ dtc) ₂] ₂ ·L | Fe | Et | DABCO | 2.5241(3) | 2.4024(3) | 2.4024(3) | 2.5241(3) | — |
| 13 | [M ^{II} (R ₂ dtc) ₂] ₂ ·L | Cd | Pr ⁱ | DABCO | 2.6011(4) | 2.5907(4) | 2.5907(4) | 2.6011(4) | — |
| 15 | [M ^{II} (R ₂ dtc) ₂] ₂ ·L | Hg | Pr ⁿ | DMP | 2.7300(11) | 2.5411(10) | 2.9420(11) | 2.4207(10) | — |

* The axial bond.

Table 2. Angles in metal(II) dithiocarbamates, both free and coordinated to nitrogen-containing ligands

| Complex | Angle/deg | | | | |
|-----------|------------|------------|-------------|-------------|----------|
| | α | β | γ | δ | ψ^* |
| 2 | 76.90(3) | 77.06(3) | 164.84(3) | 173.00(3) | 160.9 |
| 3 | 66.67(3) | 70.29(3) | 143.80(3) | 157.64(4) | 143.8 |
| 4 | 69.73(2) | 63.14(2) | 143.41(2) | 156.27(2) | 144.37 |
| 10 | 69.064(6) | 69.064(6) | 150.702(10) | 163.779(11) | 148.94 |
| 11 | 71.155(13) | 71.155(13) | 148.32(3) | 161.23(3) | 146.45 |
| 12 | 72.601(10) | 72.601(10) | 146.507(18) | 159.740(19) | 144.78 |
| 13 | 69.426(13) | 69.426(13) | 157.31(2) | 162.50(2) | 154.65 |
| 15 | 68.99(3) | 66.52(3) | 141.14(4) | 158.01(3) | 137.84 |

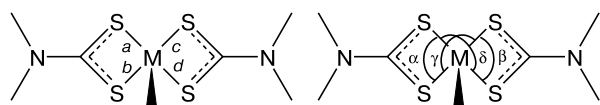
* The dihedral angle between the NCS₂M planes.

[[Hg(Prⁿ₂dtc)₂]₂·DMP]·(C₆₀)₅·(PhCl)₂ (**15**),* are formed only with dithiocarbamates contain long alkyl substituents (R = Prⁿ or Buⁿ).

2. Crystal structures of complexes

2.1. Complexes with dinuclear metal dithiocarbamates

Selected geometric parameters of M^{II}(Et₂dtc)₂ and the lengths of the van der Waals contacts in C₆₀ complexes are given in Tables 1–4. The molecular structures of M^{II}(Et₂dtc)₂ are shown in Fig. 1.



The [Cu^{II}(EtMe₂dtc)₂]₂·C₆₀ (**1**), [Cu^{II}(Et₂dtc)₂]₂·C₆₀ (**2**), [Cd(Et₂dtc)₂]₂·C₆₀ (**3**), and [Hg^{II}(Et₂dtc)₂]₂·C₆₀ (**4**) complexes have layered structures. The fullerene and metal

* Complexes of C₆₀ with dialkyldithiocarbamates (R = Prⁿ or Buⁿ, M = Zn or Cd) coordinated to DMP are beyond the scope of the present study.

Table 3. Van der Waals contacts between fullerenes and dithiocarbamates in complexes **2–4**, **10–13**, and **15**

| Complex | Distance/Å | | | | | |
|-----------|---------------------|-------|----------------------|----------------------|----------------------|----------------------|
| | N _L ...M | M...M | M...C _{C60} | S...C _{C60} | N...C _{C60} | H...C _{C60} |
| 2 | — | 3.529 | 3.269, 3.307 | 3.52—, 3.89 | 3.68—, 3.81 | 2.84—, 2.94 |
| 3 | — | 3.802 | 3.587, 3.592 | 3.51—, 3.80 | 3.52—, 3.77 | 2.86—, 3.13 |
| 4 | — | 3.939 | 3.569, 3.615 | 3.497—, 3.698 | 3.75 | 2.891 |
| 10 | 2.3419 | 7.259 | 3.461, 3.461 | 3.60—, 3.75 | 3.63—, 3.71 | 2.87—, 3.02 |
| 11 | 2.241(2) | 7.077 | 3.520, 3.520 | 3.59—, 3.80 | 3.583 | 2.826 |
| 12 | 2.1655(16) | 6.922 | 3.560, 3.560 | 3.61—, 3.83 | 3.56—, 3.63 | 2.82—, 3.06 |
| 13 | 2.362(2) | 7.322 | 3.460, 3.460 | 3.55—, 3.94 | 3.77 | >3.4 |
| 15 | 2.508(4) | 6.530 | 4.061, 4.320 | 3.443—, 3.448 | 3.243—, 3.707 | >3.30 |

dithiocarbamate molecules in these structures are completely ordered.

In the [Cu^{II}(Et₂dtc)₂]₂·C₆₀ complex (**2**), the close-packed layers with the square arrangement of the fullerene molecules alternate with the {Cu^{II}(Et₂dtc)₂]₂ layers (Fig. 2). Each C₆₀ molecule in the layer is surrounded by four adjacent C₆₀ molecules along the diagonals to the *bc* plane; the distance between the centers of the fullerene molecules is 10.02 Å (see Fig. 2, *a*). There are shortened C...C van der Waals contacts between the fullerene molecules (3.329–3.466 Å, the sum of the van der Waals radii of two sp²-hybridized carbon atoms is 3.42 Å).⁴¹ The distance between the centers of the fullerene molecules (10.02 Å) is similar to the corresponding distance in C₆₀ at 153 K (9.94 Å).⁴²

The projection of the Cu^{II}(Et₂dtc)₂ layer onto the C₆₀ layer is shown in Fig. 2, *a*. The central CuS₄ fragment is located above the C₆₀ sphere, whereas the Et groups

Table 4. Geometric parameters characterizing the mutual arrangement of the dithiocarbamate and fullerene fragments in the crystal structures of complexes **2–4**, **10–13**, and **15**

| Complex | ψ^a /deg | Packing mode of fullerenes | Number of adjacent C_{60} molecules | Distance between the centers of $C_{60}/\text{\AA}$ | $d_{\text{vdw}}(C\dots C)^b/\text{\AA}$ ($<3.45 \text{\AA}$) |
|-----------|-------------------|-------------------------------|--|--|---|
| 2 | 9.8, 13.6 | Square layers | 4 | 10.020($\times 4$), 10.250($\times 2$) | 3.329–3.466 |
| 3 | 0.8, 8.2 | Square layers | 4 | 9.990($\times 4$), 10.536($\times 2$) | 3.328–3.770 |
| 4 | 1.0, 10.2 | Square layers | 4 | 9.987($\times 4$), 10.556($\times 2$) | 3.229–3.393 |
| 10 | 5.7, 5.7 | Square layers | 4 | 10.004($\times 4$), 10.458($\times 2$) | 3.365–3.367 |
| 11 | 5.0, 5.0 | Square layers | 4 | 10.001($\times 4$), 10.441($\times 2$) | 3.369, 3.369 |
| 12 | 4.6, 4.6 | Square layers | 4 | 9.938($\times 4$), 10.349($\times 2$) | 3.311–3.399 |
| 13 | 16.8, 16.8 | Layers | 0 | 10.113($\times 4$), 11.716($\times 2$) | >3.57 |
| 15 | 19.4 ^c | Three-dimensional | 6–7 ^d | 9.714–10.281 | 3.078–3.470 |

^a The dihedral angle between the planes of NCS_2M and the hexagons of C_{60} .

^b Van der Waals contacts between fullerenes.

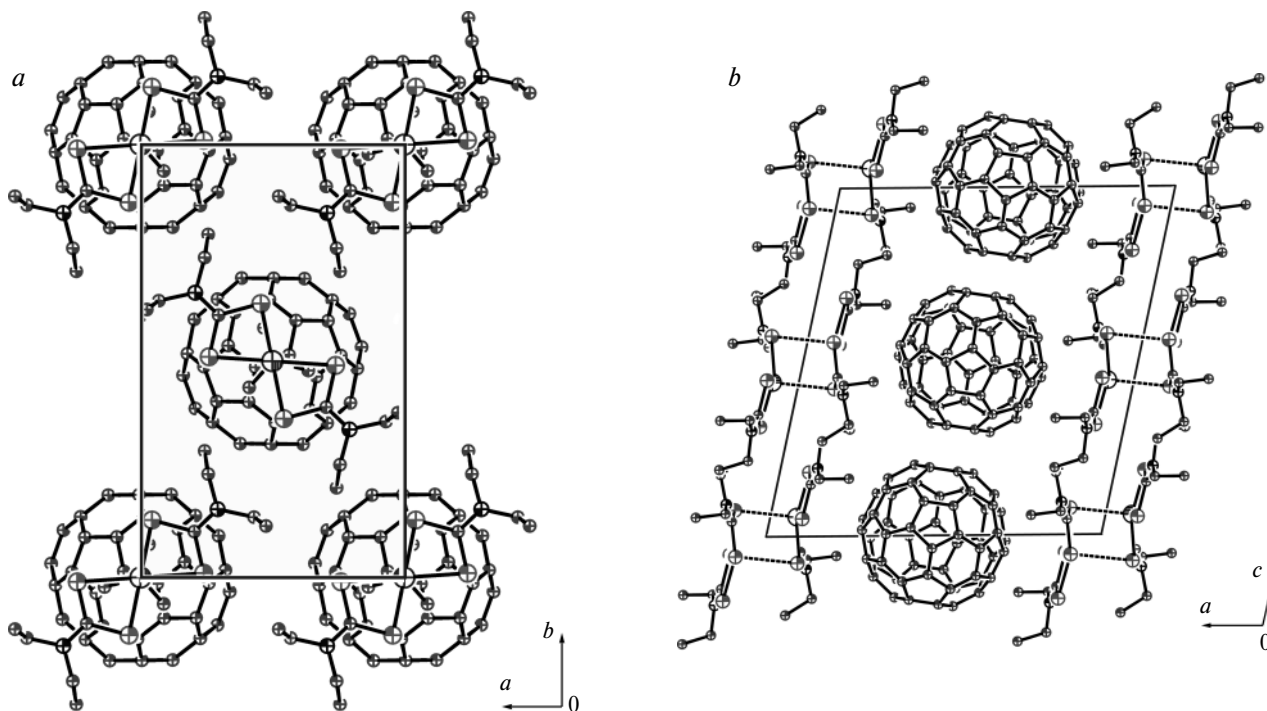
^c For one hexagon of C_{60} .

^d In complex **15**, there are three independent C_{60} molecules; two of these molecules are surrounded by six C_{60} molecules; one C_{60} molecule, by seven C_{60} molecules.

occupy the cavities in the fullerene layer. The $\{\text{Cu}^{\text{II}}(\text{Et}_2\text{dtc})_2\}_2$ complexes are packed in the layers in a herringbone fashion (see Fig. 2, *a*). The carbon atoms of one 6–6 bond in C_{60} are involved in $\text{Cu}\dots\text{C}_{C_{60}}$ contacts (3.269 and 3.307 \AA). These contacts are substantially longer than the analogous $\text{Cu}\dots\text{C}_{C_{60}}$ contacts in the fullerenes complexes with copper(II) octaethyl- and tetraphenylporphyrinates (2.88–3.02 \AA),^{13,14} which is indicative of a weak coordination between the metal atom and fullerene. In this complex, there are van der Waals contacts between $\text{Cu}^{\text{II}}(\text{Et}_2\text{dtc})_2$ and C_{60} (see Tables 1–3).

Noteworthy are the $\text{H}\dots\text{C}$ contacts between the ethyl substituents of $\{\text{Cu}^{\text{II}}(\text{Et}_2\text{dtc})_2\}_2$ and C_{60} (2.845–2.938 \AA), which, apparently, play an important role in the ordering of C_{60} molecules. These contacts are formed because the C–H bonds of the ethyl substituents are directed toward the carbon atoms of C_{60} implying C–H $\dots\pi$ interactions. Analogous contacts were found in other layered complexes as well.

In the starting dithiocarbamate $\{\text{Cu}^{\text{II}}(\text{Et}_2\text{dtc})_2\}_2$, the Cu^{II} atoms are in a square-pyramidal environment. Four equatorial Cu–S bonds are short (aver., 2.3117 \AA),

**Fig. 2.** Crystal structure of **2** projected along the crystallographic \bar{a} (*a*) and \bar{b} (*b*) axes.

whereas the axial Cu—S bond is longer (2.844(1) Å).²¹ In complex **2**, the axial Cu—S bond in {Cu^{II}(Et₂dtc)₂}₂ is elongated to 3.030(2) Å. The elongation of this bond can be associated with the weak coordination of the Cu^{II} atom to fullerene. In complex **2**, the arrangement of the Et groups in {Cu^{II}(Et₂dtc)₂}₂ also differs from that in the starting dithiocarbamate Cu^{II}(Et₂dtc)₂. Thus, the ethyl groups at each nitrogen atom in the starting dithiocarbamate point in the opposite directions,²¹ whereas three of four Et substituents of Cu^{II}(Et₂dtc)₂ in complex **2** are directed toward the fullerene layer.

In the [Cu^{II}(EtMedtc)₂]₂·C₆₀ complex (**1**), the C₆₀ molecules form close-packed hexagonal layers, in which each fullerene molecule is linked to six adjacent C₆₀ molecules by van der Waals contacts (distances between the centers of C₆₀ are 9.89 and 10.02 Å).³² The C₆₀ molecules in complex **1** are more close-packed compared to those in **2** because only two Et substituents in {Cu^{II}(EtMedtc)₂}₂ protrude into the cavities in the fullerene layer. The replacement of two Et groups with methyl substituents results in the formation of the closer packing of the {Cu^{II}(EtMedtc)₂}₂ molecules in the donor layers. The Cu...C₆₀ distances are 3.334 and 3.379 Å.

In the [Cd(Et₂dtc)₂]₂·C₆₀ (**3**) and [Hg(Et₂dtc)₂]₂·C₆₀ (**4**) complexes, the fullerene molecules have a square arrangement in the layers; the distance between the centers of the fullerene molecules along the diagonals to the *bc* plane is 9.99 Å. The efficient packing of {M(Et₂dtc)₂}₂ and C₆₀ in the crystal structure is achieved because the dinuclear dithiocarbamate adopts an open-book shape (see Fig. 1). The cavity formed by four MS₂CNEt₂ fragments ideally matches the C₆₀ molecule (Fig. 3, *a*). The M...C₆₀ contacts are formed with the involvement of two

carbon atoms belonging to the 6—6 bond of C₆₀. These distances (3.587 and 3.592 Å in **3** and 3.569 and 3.615 Å in **4**) are longer than those in complexes **1** and **2**, *i.e.*, the coordination of the metal atom to fullerene is virtually absent in complexes **3** and **4**. The cocrystallization of {Cd(Et₂dtc)₂}₂ with C₆₀ leads to an elongation of the axial bond in dithiocarbamate from 2.812 Å in the starting compound^{22,23} to 2.877 Å in **3**. In complexes **3** and **4**, only two of four Et groups of M(Et₂dtc)₂ are directed inside the fullerene layer (starting compound {Cd(Et₂dtc)₂}₂ adopts an analogous conformation).^{22,23}

In spite of the similarity of the crystal structures of **1**, **2** and **3**, **4**, the character of interactions between the metal dithiocarbamates and C₆₀ in these structures is substantially different. This is primarily associated with the difference in the angles between the MS₂CN planes in dithiocarbamates. In dithiocarbamates {Cu^{II}(EtMedtc)₂}₂ and {Cu^{II}(Et₂dtc)₂}₂, the axial Cu—S bond is relatively long and, as a consequence, the central Cu^{II}(S₂CN)₂ fragment in these compounds is more planar (dihedral angle between the Cu^{II}S₂CN planes is 158.6° (**1**) and 160.9° (**2**)). In dithiocarbamates {M(Et₂dtc)₂}₂ (M = Cd or Hg) linked by the short axial M—S bond, this angle is 143.8° (**3**) and 144.4° (**4**). The more planar Cu(S₂CN)₂ fragment in **1** and **2** is favorable for the formation of shorter Cu...C₆₀ contacts compared to the analogous M...C₆₀ contacts in **3** and **4**. However, the more concave shape of the M(Et₂dtc)₂ fragment (M = Cd or Hg) better matches the spherical shape of C₆₀, because the dihedral angles between two adjacent hexagons of C₆₀ (138.5°) and the MS₂CN planes in Cd and Hg^{II} dithiocarbamates have close values (see Fig. 3, *a*). This leads to more efficient interactions between their π systems (corresponding dihedral angles between the MS₂CN planes and the hexagons of C₆₀ are as small as 0.8 and 8.2° in **3** and 1.0 and 10.2° in **4**). The corresponding dihedral angles in **1** and **2** are substantially larger (9.8, 13.6° and 9.5, 12.6°, respectively).

2.2. Complex of C₆₀ with Zn(Et₂dtc)₂

The Zn(Et₂dtc)₂·C₆₀·(PhCl)_{0.5}·(C₆H₆)_{0.5} complex (**16**) has an unusual three-dimensional framework structure consisting of C₆₀ molecules with channels running along the \bar{a} axis. The channels are occupied by the Zn(Et₂dtc)₂ and solvent molecules (Fig. 4). Each C₆₀ molecule is surrounded by six adjacent C₆₀ molecules; the distances between the centers of these molecules are in the range 9.74–9.93 Å, which are similar or shorter than the corresponding distances in C₆₀.⁴² The shortened C...C van der Waals contacts between the adjacent fullerene molecules are 3.250–3.360 Å. In complex **16**, the Zn^{II} atoms in Zn(Et₂dtc)₂ are in a pseudotetragonal environment. Due to the nonplanar structure, only one-half

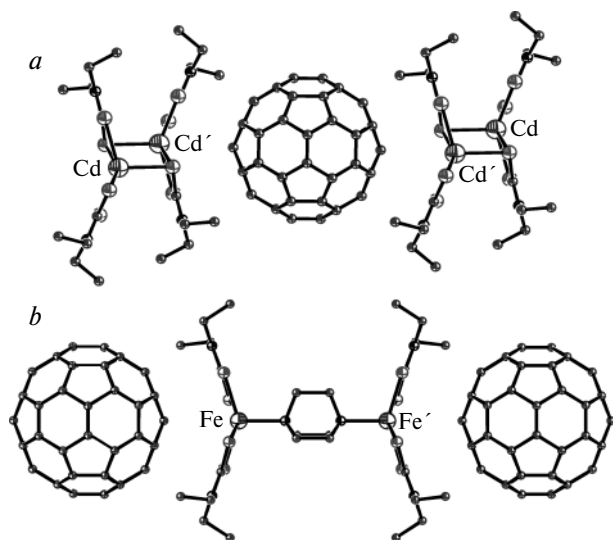


Fig. 3. Mutual arrangement of {Cd(Et₂dtc)₂}₂ and C₆₀ in complex **3** (*a*) and the mutual arrangement of {Fe^{II}(Et₂dtc)₂}₂·DABCO and C₆₀ in complex **11** (*b*).

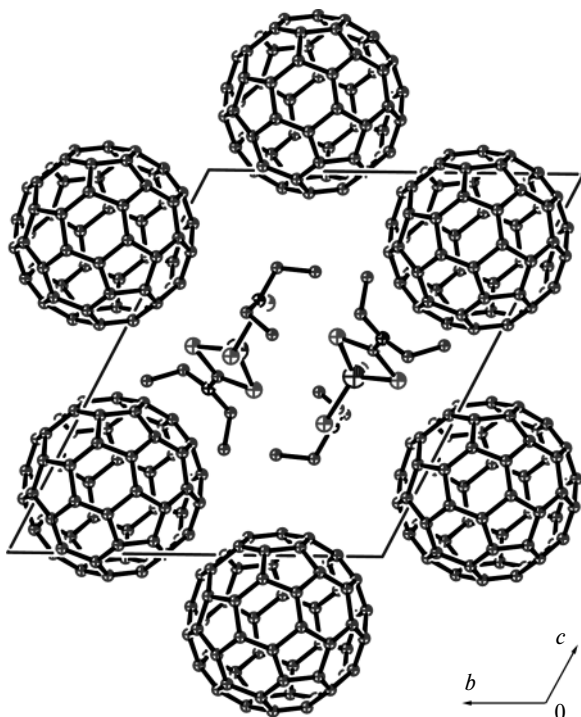


Fig. 4. Crystal structure of **16** projected along the crystallographic \bar{a} axis. The $\text{Zn}(\text{Et}_2\text{dtc})_2$ and solvent molecules are located in the channels. Solvent molecules are omitted.

of the $\text{Zn}(\text{Et}_2\text{dtc})_2$ molecule forms van der Waals contacts with C_{60} , but π – π interactions with C_{60} are absent. The shortest $\text{Zn}\dots\text{C}_{\text{C}_{60}}$ distance is 3.659 Å, which is similar to the lengths of the $\text{M}\dots\text{C}_{\text{C}_{60}}$ contacts in **3** and **4**.

2.3. Complexes of C_{60} with coordinated metal dithiocarbamates

The bidentate ligands DABCO and DMP (L) are coordinated to two metal dithiocarbamate molecules (Zn, Cd, Hg, Mn, and Fe) to form dinuclear dithiocarbamates $\{\text{M}^{\text{II}}(\text{R}_2\text{dtc})_2\}_2 \cdot \text{L}$. Their molecular structures are presented in Fig. 1. The bond lengths and bond angles are given in Tables 1–3. The axial $\text{M}-\text{N}_{\text{L}}$ bond lengths in these dithiocarbamates are substantially smaller than the equatorial $\text{M}-\text{S}$ bond lengths and are increased in the order: Zn (2.14 Å) < Fe (2.16 Å) < Mn (2.24 Å) < Cd (2.34–2.36 Å) < Hg (2.51 Å). The average lengths of the equatorial $\text{M}-\text{S}$ bonds increase in approximately the same order: Fe (2.46 Å) \leq Zn (2.47 Å) < Mn (2.54 Å) < Cd (2.60–2.62 Å) < Hg (2.66 Å). Therefore, it is clearly seen that the $\text{M}-\text{N}_{\text{L}}$ and $\text{M}-\text{S}$ bond lengths increase with increasing covalent radius of the central metal atom in dithiocarbamates: Zn (0.74 Å), Fe^{II} (0.74 Å), Mn^{II} (0.80 Å), Cd (0.97 Å), and Hg^{II} (1.10 Å).⁴³

The coordinated dinuclear dithiocarbamates in the complexes with fullerenes have different structures

depending on the nature of the substituent (R) and the ligand (L). In $\{\text{M}(\text{Et}_2\text{dtc})_2\}_2 \cdot \text{DABCO}$ (**10**–**12**), the $\text{M}(\text{Et}_2\text{dtc})_2$ fragments are located exactly one above another. In $\{\text{Cd}(\text{Pr}^i_2\text{dtc})_2\}_2 \cdot \text{DABCO}$ (**13**) containing the bulkier Pr^i substituents, the $\text{Cd}(\text{Pr}^i_2\text{dtc})_2$ fragments are located at an angle of 69.4° to each other. In $\{\text{Hg}^{\text{II}}(\text{Pr}^n_2\text{dtc})_2\}_2 \cdot \text{DMP}$ (**15**), the $\text{Hg}^{\text{II}}(\text{Pr}^n_2\text{dtc})_2$ fragments are shifted with respect to each other by ~2.9 Å. In spite of the fact that HMTA is a tetradentate ligand, this ligand gives rise only to coordinated mononuclear dithiocarbamate $\{\text{Zn}(\text{Et}_2\text{dtc})_2\} \cdot \text{HMTA}$ in the case of complex **14** (see Fig. 1).

The C_{60} complexes with $\{\text{M}^{\text{II}}(\text{Et}_2\text{dtc})_2\}_2 \cdot \text{DABCO}$ ($\text{M} = \text{Cd}$ (**10**), Mn (**11**), or Fe (**12**) (Fig. 5)), $\{\text{Cd}(\text{Pr}^i_2\text{dtc})_2\}_2 \cdot \text{DABCO}$ (**13**), and $\{\text{Zn}(\text{Et}_2\text{dtc})_2\} \cdot \text{HMTA}$ (**14**) have layered structures. The C_{60} molecules are ordered in all these structures (except for **13**) because the book shape of the dithiocarbamate molecules is sterically compatible with the spherical shape of C_{60} (see Fig. 3, b).

In complexes **10**, **11**, **12**, and **14**, each C_{60} molecule in the layers is surrounded by four C_{60} molecules; the distances between the centers of the fullerene molecules are 10.004 (**10**), 10.001 (**12**), 9.94 (**11**) (see Fig. 5), and 9.92–9.94 Å (**14**) and are similar to the corresponding distances in C_{60} .⁴² As a result of the close packing in the layer, the C...C van der Waals contacts between the fullerene molecules are in the range of 3.296–3.385 Å (see Table 3). The distance between the centers of fullerene molecules depends on the nature of the central metal atom, to be more precise, on the average length of the equatorial $\text{M}-\text{S}$ bonds, and increases in the series $\text{Cd} > \text{Mn} > \text{Fe} > \text{Zn}$. The structure of the C_{60} complex with $\{\text{Cd}(\text{Pr}^i_2\text{dtc})_2\}_2 \cdot \text{DABCO}$ (**13**) consists of layers formed by the isolated C_{60} molecules. The distance between the centers of these molecules is 10.11 Å. In this structure, there are no van der Waals contacts between C_{60} . This is due to the fact that four Me groups of $\text{Cd}(\text{Pr}^i_2\text{dtc})_2$ in complex **13** protrude into the fullerene layer, thus pushing the C_{60} molecules apart, whereas only two Et groups of $\text{M}^{\text{II}}(\text{Et}_2\text{dtc})_2$ in complexes **10**–**12** and **14** are located in the fullerenes layer. Therefore, the length of the alkyl substituents and the nature of metal in dithiocarbamates determine the distances between the C_{60} molecules in these layers.

The projection of the $\{\text{Fe}^{\text{II}}(\text{Et}_2\text{dtc})_2\}_2 \cdot \text{DABCO}$ layer onto the C_{60} layer in complex **11** is shown in Fig. 5. The central FeS_4 fragment is located above the C_{60} sphere, so that the Fe^{II} atom approaches the 6–6 bond of C_{60} and forms $\text{Fe}\dots\text{C}_{\text{C}_{60}}$ contacts (3.56 Å). In other layered complexes, metal dithiocarbamates are arranged in a similar fashion. The $\text{M}\dots\text{C}_{\text{C}_{60}}$ distance is 3.46 Å in **10** and **15**, 3.52 Å in **12**, and 3.53–3.58 Å in **14**, which is indicative of the absence of coordination bonding between the metal atom of dithiocarbamate and fullerene.

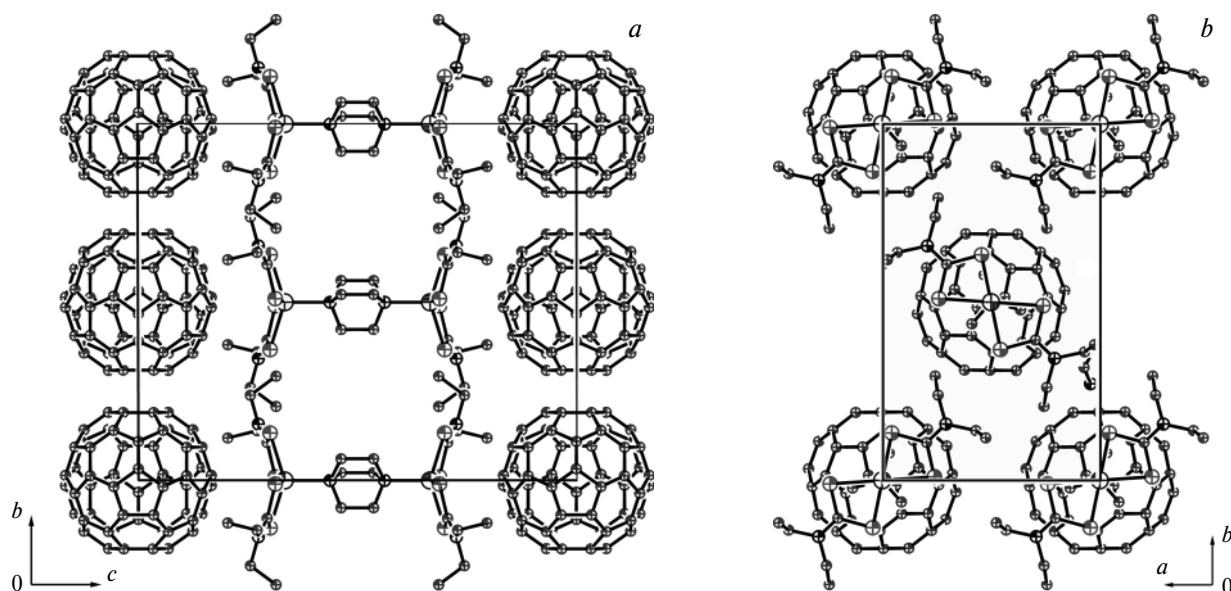


Fig. 5. Crystal structure of **11** projected along the crystallographic \bar{a} (*a*) and \bar{c} (*b*) axes. The DABCO molecules located in the $\{\text{Fe}^{\text{II}}(\text{Et}_2\text{dtc})_2\}_2 \cdot \text{DABCO}$ layer are omitted.

The structure of **15** is three-dimensional and contains large vacancies occupied by the $\{\text{Hg}(\text{Pr}^n_2\text{dtc})_2\}_2 \cdot \text{DMP}$ and solvent molecules (Fig. 6). This is responsible for the unusual composition of the complex, in which there are five C_{60} molecules per coordinated dithiocarbamate mol-

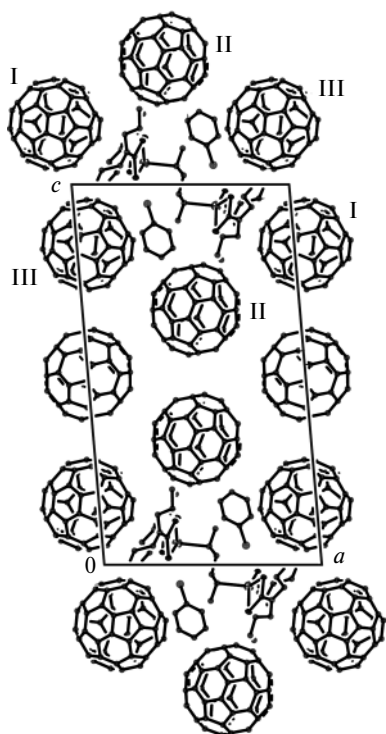


Fig. 6. Crystal structure of **15** projected along the crystallographic \bar{b} axis. Only one orientation of the disordered chlorobenzene and type III fullerene molecules is shown.

ecule. Complex **15** contains three crystallographically independent C_{60} molecules. The C_{60} molecules of one type form van der Waals contacts with the central $\text{Hg}(\text{Pr}^n_2\text{dtc})_2$ fragment, as was observed in complexes **10–13** and **14** (see Fig. 6, type I). The C_{60} molecules of the second type (see Fig. 6, type II) are located between the *n*-propyl substituents of $\text{Hg}(\text{Pr}^n_2\text{dtc})_2$. The C_{60} molecules of the third type (see Fig. 6, type III) are not involved in van der Waals contacts with $\{\text{Hg}(\text{Pr}^n_2\text{dtc})_2\}_2 \cdot \text{DMP}$, and form such contacts only with PhCl. As a consequence, these C_{60} molecules are disordered. Each C_{60} molecule is surrounded by six–seven adjacent C_{60} molecules. These molecules form a close packing and are involved in numerous $\text{C}\dots\text{C}$ van der Waals contacts (3.078–3.470 Å). The Hg^{II} atom, like the metal atoms in the above-considered complexes, approaches the 6–6 bond of C_{60} ; the $\text{Hg}\dots\text{C}_{60}$ distances are in the range of 4.06–4.32 Å.

The $\text{M}(\text{R}_2\text{dtc})_2$ fragments in $\{\text{M}(\text{R}_2\text{dtc})_2\}_2 \cdot \text{DABCO}$ and $\{\text{Zn}(\text{Et}_2\text{dtc})_2\} \cdot \text{HMTA}$ are book-shaped; the dihedral angles between the MS_2CN planes are in the range of 144.78–148.94° (see Table 2). These angles are similar to the dihedral angle between the planes of two hexagons in the C_{60} molecule, resulting in good steric compatibility between the shapes of the dithiocarbamate and C_{60} molecules (see Fig. 3, *b*). As a consequence, there are efficient interactions between their π systems (dihedral angles between the MS_2CN planes and the hexagons of C_{60} are as small as 4.56–5.70°, the van der Waals contacts are smaller than the sum of the van der Waals radii of the corresponding atoms). If the dihedral angles between the MS_2CN planes are smaller (137.8°) or larger (154.6°) (for example, in $\{\text{Hg}(\text{Pr}^n_2\text{dtc})_2\}_2 \cdot \text{DMP}$ (**15**) and $\{\text{Cd}(\text{Pr}^1_2\text{dtc})_2\}_2 \cdot \text{DABCO}$ (**13**), respectively), π – π inter-

actions are weaker (corresponding dihedral angles are 16.76–19.43°, see Tables 2 and 3). It should be noted that it is the structures of **13** and **15**, in which the fullerene molecules are disordered.

3. Magnetic properties of C₆₀ complexes with Cu^{II}, Mn^{II}, and Fe^{II} dithiocarbamates

The ESR spectroscopy is a rather sensitive technique allowing the detection of changes in the environment of Cu^{II} atoms associated with the complex formation of Cu(R₂dtc)₂ with C₆₀. The ESR spectrum of {Cu^{II}(Et₂dtc)₂}₂·C₆₀ (**2**) (Fig. 7, *b*) substantially differs from that of the starting dithiocarbamate Cu(Et₂dtc)₂ (Fig. 7, *a*). These changes are apparently attributed to a weak coordination of Cu^{II} atoms to C₆₀, resulting in an elongation of the axial Cu—S bond in {Cu^{II}(Et₂dtc)₂}, the flattening of the central Cu^{II}(S₂CN)₂ fragment, and an increase in the asymmetry of the environment of the Cu^{II} atoms. Analogous ESR spectra are observed for C₆₀ complexes with other Cu^{II}-containing dithiocarbamates (**1**, **7**, and **8**). The magnetic susceptibility of complexes **1** and **2** in the temperature range of 10–300 K is described

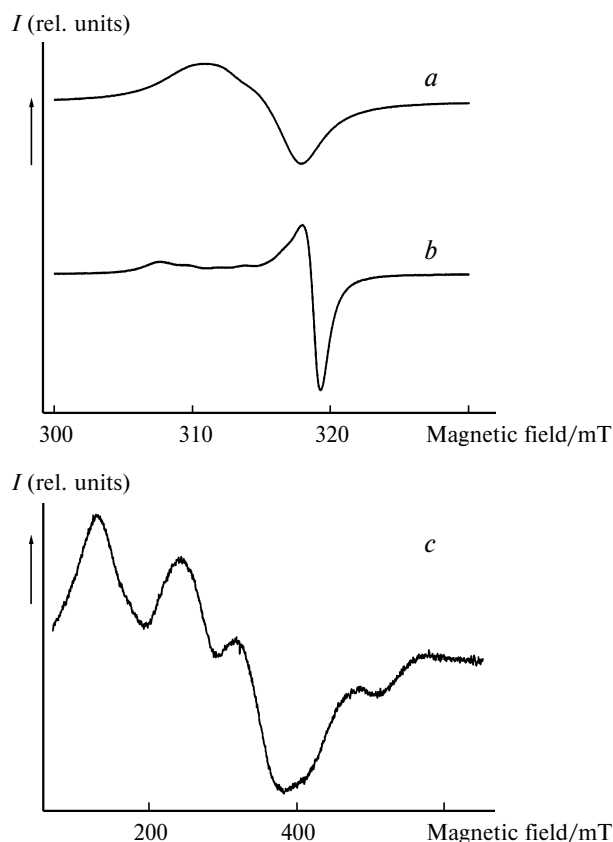


Fig. 7. ESR spectra of the starting dithiocarbamate {Cu^{II}(Et₂dtc)₂}₂ (*a*), the {Cu^{II}(Et₂dtc)₂}₂·C₆₀ complex (**2**) (*b*), and the {Mn^{II}(Et₂dtc)₂}₂·C₇₀ complex (**6**) (*c*) at room temperature; *I* is the intensity of the signal.

by the Curie–Weiss law with the negative Weiss constants of –2.5 K (**1**) and –2.0 K (**2**), which is indicative of a weak antiferromagnetic spin coupling between Cu^{II} in {Cu(R₂dtc)₂}₂. The weak coupling is attributable to the longer axial Cu—S bond (2.787(1) Å in **1** and 3.030(2) Å in **2**), through which the magnetic coupling is transferred.

The starting dinuclear dithiocarbamate {Fe^{II}(Et₂dtc)₂}₂ gives the ESR signal with *g* = 2.0708 and Δ*H* = 61.6 mT; Mn^{II}(Et₂dtc)₂ containing Mn^{II} in a distorted octahedral environment⁴⁰ gives the ESR signal with *g* = 2.0115 and the width Δ*H* = 61.8 mT.

The {Fe^{II}(Et₂dtc)₂}₂·C₆₀ complex gives no ESR signals. The complicated ESR spectrum is observed for the {Mn^{II}(Et₂dtc)₂}₂·C₇₀ complex (**6**). This spectrum shows several components in the magnetic field from 50 to 500 mT (see Fig. 7, *c*). The changes in the ESR spectrum of Mn^{II}(Et₂dtc)₂ upon the complex formation with fullerene are apparently associated with the changes in the local environment of Mn^{II} in going from the polynuclear structure of the starting donor⁴⁰ to dinuclear structure in **6**. Analogous ESR spectra are observed for other dinuclear Mn^{II} complexes.^{44,45} The absence of ESR signals characteristic⁴⁶ of the radical anions of C₆₀ and C₇₀ in both complexes is indicative of the absence of the charge transfer from iron(II) and manganese(II) dithiocarbamates to fullerene.

At 300 K, the magnetic moments of complexes **5** and **6** are 6.00 and 7.75 μ_B (Fig. 8, *a*, *b*), respectively, which is evidence of the high-spin state of Fe^{II} and Mn^{II} in these complexes (calculated magnetic moments for the system consisting of two uncoupled spins *S* = 2 and *S* = 5/2 are 6.93 and 8.37 μ_B, respectively). The magnetic susceptibility of the complexes in the temperature range of 200–300 K can be described by the Curie–Weiss law with the negative Weiss constants of –250 K (**5**) and –96 K (**6**), and the maxima of the magnetic susceptibility are achieved already at 110 K (**5**) and 46 K (**6**). This is indicative of a very strong antiferromagnetic spin coupling between Fe^{II} and Mn^{II} associated, most likely, with the dinuclear structure of {M^{II}(Et₂dtc)₂}₂ (*M* = Fe or Mn) in these complexes. Unlike {Cu^{II}(Et₂dtc)₂}₂ containing the long axial Cu—S bond, the starting dithiocarbamate {Fe^{II}(Et₂dtc)₂}₂ has the short axial Fe—S bond (2.437 Å).²⁴ Upon the complex formation with fullerenes, the short axial M—S bond should be retained in {M^{II}(Et₂dtc)₂}₂ (*M* = Fe or Mn), as was observed in complexes **3** and **4**. This should lead to a strong antiferromagnetic spin coupling between the metal atoms.

Upon the formation of {M^{II}(Et₂dtc)₂}₂·DABCO, the metal atoms in **11** (Fe^{II}) and **12** (Mn^{II}) are separated by the DABCO ligand. The distances between the metal atoms are 6.922 and 7.077 Å, respectively. The ESR spectrum of **12** contains several components at 171, 262, 460, and 646 mT and is similar to the spectrum of **6** and the spectra of a number of other dinuclear Mn^{II} com-

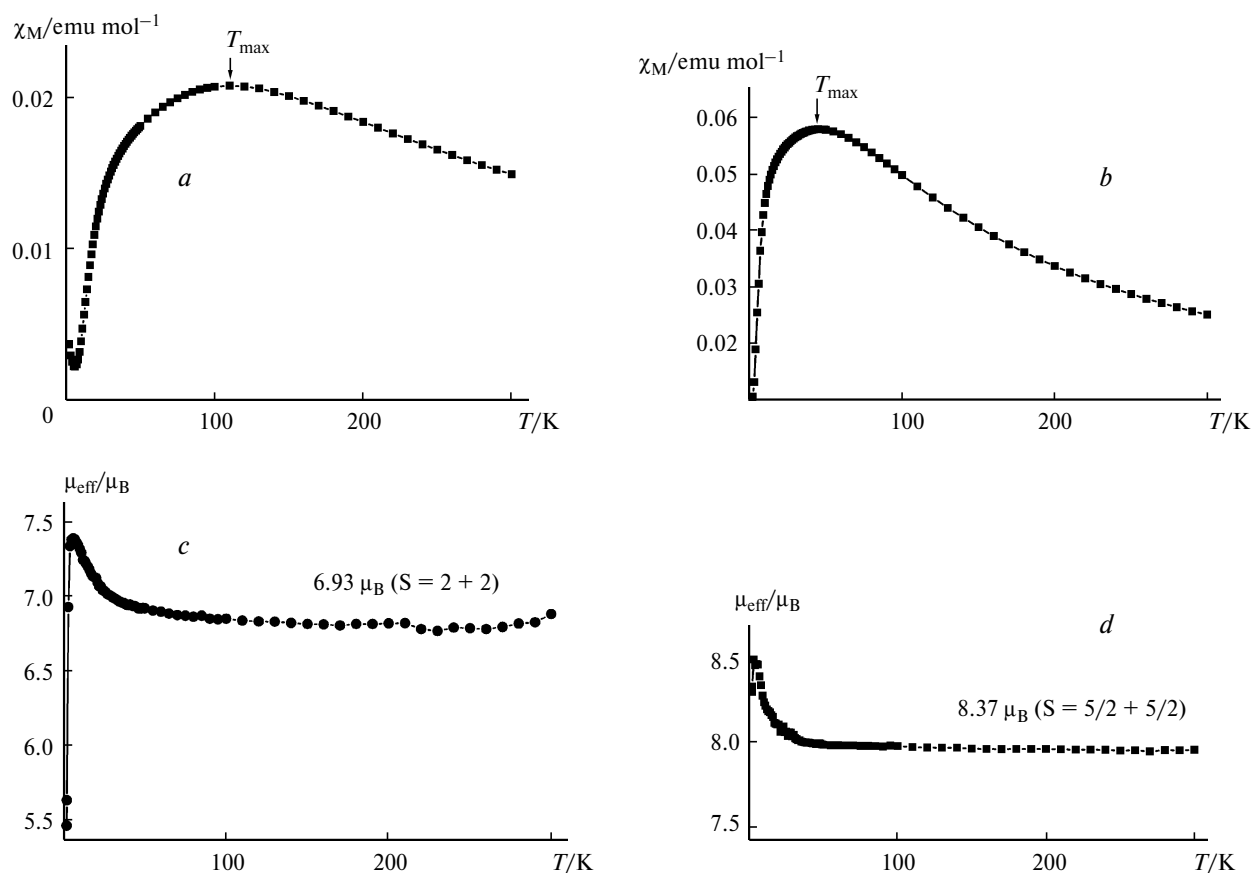


Fig. 8. Data from magnetic measurements for the complexes in the temperature range of 1.9–300 K: the molar magnetic susceptibilities of $\{\text{Fe}^{\text{II}}(\text{Et}_2\text{dtc})_2\}_2 \cdot \text{C}_{60}$ (**5**) (a) and $\{\text{Mn}^{\text{II}}(\text{Et}_2\text{dtc})_2\}_2 \cdot \text{C}_{70}$ (**6**) (b). The magnetic moments of $[\{\text{Fe}^{\text{II}}(\text{Et}_2\text{dtc})_2\}_2 \cdot \text{DABCO}] \cdot \text{C}_{60} \cdot (\text{DABCO})_2$ (**11**) (c) and $[\{\text{Mn}^{\text{II}}(\text{Et}_2\text{dtc})_2\}_2 \cdot \text{DABCO}] \cdot \text{C}_{60} \cdot (\text{DABCO})_2$ (**12**) (d).

plexes.^{44,45} This spectrum is associated with the exchange interaction between two Mn^{II} atoms in $\{\text{Mn}(\text{Et}_2\text{dtc})_2\}_2 \cdot \text{DABCO}$. Although $\text{Mn}^{\text{II}}(\text{Et}_2\text{dtc})_2$ and $\text{Fe}^{\text{II}}(\text{Et}_2\text{dtc})_2$ are rather strong donors (oxidation potentials of $\text{M}^{\text{III}}(\text{dtc})_3^{1-/0}$ are -0.08 and -0.37 V, respectively²⁷), these dithiocarbamates cannot reduce fullerene (first reduction potential of C_{60} is -0.485 V;⁴⁷ all potentials were measured with respect to Ag/AgCl). Actually, both complexes exhibit no ESR signals of the $\text{C}_{60}^{\cdot -}$ radical anion, which is evidence of the absence of the charge transfer to the fullerene molecule. Earlier, it has been demonstrated¹² that the charge transfer in the C_{60} and C_{70} complexes with manganese(II) tetraphenylporphyrin is also absent.

The temperature dependences of the magnetic moments of **11** and **12** are shown in Fig. 8, c, d. At 300 K, the magnetic moments are 6.88 and $8.23 \mu_{\text{B}}$, respectively, and are similar to those calculated for the system consisting of two uncoupled spins $S = 2$ ($6.93 \mu_{\text{B}}$) and $S = 5/2$ ($8.37 \mu_{\text{B}}$). This is indicative of the high-spin state of the metal atoms. The temperature dependences of the magnetic susceptibility of **11** and **12** in the range of 50–300 K can be described by the Curie–Weiss law with the positive Weiss

constants of 1.70 and 0.35 K, respectively. At temperatures below 50 and 35 K, a slight increase in the magnetic moment is observed for both complexes; the maximum values are $8.5 \mu_{\text{B}}$ (at 3 K) and $7.4 \mu_{\text{B}}$ (at 6 K) (see Fig. 8, c, d). An increase in the magnetic moments along with the positive Weiss constants is evidence of the ferromagnetic spin coupling between M^{II} in $\{\text{M}^{\text{II}}(\text{Et}_2\text{dtc})_2\}_2 \cdot \text{DABCO}$. Apparently, the DABCO ligand with the short N...N distance (2.594 \AA) can provide the magnetic coupling between the M^{II} atoms. Apparently, this magnetic coupling has only a short-range order (within coordinated dithiocarbamate $\{\text{M}^{\text{II}}(\text{Et}_2\text{dtc})_2\}_2 \cdot \text{DABCO}$), because the dithiocarbamate molecules are isolated from each other. A lowering of the temperature below 3 and 6 K (see Fig. 8, c, d) leads to a decrease in the magnetic moments of **11** and **12**. This is apparently associated with the zero-field splitting of the spin levels of the Mn^{II} and Fe^{II} atoms in the high-spin state. This magnetic behavior is observed in coordination structures formed by hexacyanochromates and hexacyanoferrates, $\text{M}^{\text{III}}(\text{CN})_6^{3-}$, the $\text{Mn}^{\text{III}}(\text{salen})^+$ cation, or its substituted derivatives (salen is the *N,N'*-ethylenebis(salicylideneamine) dianion). In $\text{Mn}^{\text{III}}(\text{salen})^+$, the Mn^{III} atom is in the high-spin state

($S = 2$); the zero-field splitting is observed for this atom, resulting in a decrease in the magnetic moment at low temperatures.^{48–50} In compound **11**, the Fe^{II} atom has the electronic configuration identical to that of the Mn^{III} atom in the Mn^{III}(salen)⁺ cation.

Therefore, the magnetic behavior of complexes of **5** and **6** with dinuclear dithiocarbamates $\{M^{II}(\text{Et}_2\text{dtc})_2\}_2$ differs substantially from that of complexes **11** and **12** containing coordinated dithiocarbamates $\{M^{II}(\text{Et}_2\text{dtc})_2\}_2 \cdot \text{DABCO}$ ($M = \text{Fe}$ or Mn). In the former complexes, the M^{II} atoms in $\{M^{II}(\text{Et}_2\text{dtc})_2\}_2$ are separated by only one sulfur atom and the short axial M–S bond, resulting in strong antiferromagnetic interactions between M^{II}. An increase in the distance between M^{II} in $\{M^{II}(\text{Et}_2\text{dtc})_2\}_2 \cdot \text{DABCO}$ leads to a substantial weakening of the magnetic coupling, the character of the coupling changes from antiferromagnetic (**5** and **6**) to ferromagnetic (**11** and **12**).

4. Spectra of complexes in the IR, UV-Vis, and near-IR regions

The IR spectra of complexes **1–16** are superpositions of the spectra of C₆₀, donors, ligands, and solvent molecules. Individual fullerene C₆₀ is characterized by four absorption bands in the IR spectrum at 527, 577, 1182, and 1429 cm⁻¹ ($F_{1u}(1–4)$ modes, respectively). The positions of the $F_{1u}(1–3)$ modes remain unchanged in the spectra of the complexes, whereas the $F_{1u}(4)$ mode, which is most sensitive to the charge transfer to the fullerene molecule,⁵¹ is shifted by 1–8 cm⁻¹ to smaller values. The spectra of the starting divalent metal dithiocarbamates also show intense absorption bands at 1427–1435 cm⁻¹ and can contribute to the absorption at 1420–1430 cm⁻¹. In this case, it is impossible to determine the real shift of the $F_{1u}(4)$ mode upon the complex formation.

The typical absorption spectra of the complexes and donors in the UV-Vis and near-IR regions are presented in Fig. 9. The starting dithiocarbamate Cu^{II}(Et₂dtc)₂ is characterized by intense absorption with broad maxima in the visible region at 442 and 660 nm (see Fig. 9, *b*). This absorption is also observed in the spectrum of **2**, in which the main maximum appears at 437 nm (see Fig. 9, *a*). The absorption bands in the spectra of **2**, **3**, **11**, and **16** at 340 and 263 nm (± 2 nm) and the weak absorption band at ~600 nm are assigned to the intramolecular transitions in the C₆₀ molecule.⁵² The absorption band at 470 nm in the spectrum of C₆₀ is attributed to the charge-transfer band (CTB) between the adjacent fullerene molecules.^{53,54} The close packing of fullerene molecules is a necessary condition for the observation of this absorption band in the spectra of the complexes, since this band is absent in the spectra of complexes with isolated C₆₀ molecules.^{8,55} Complexes **2**, **3**, **11**, and **16** consist of close-packed

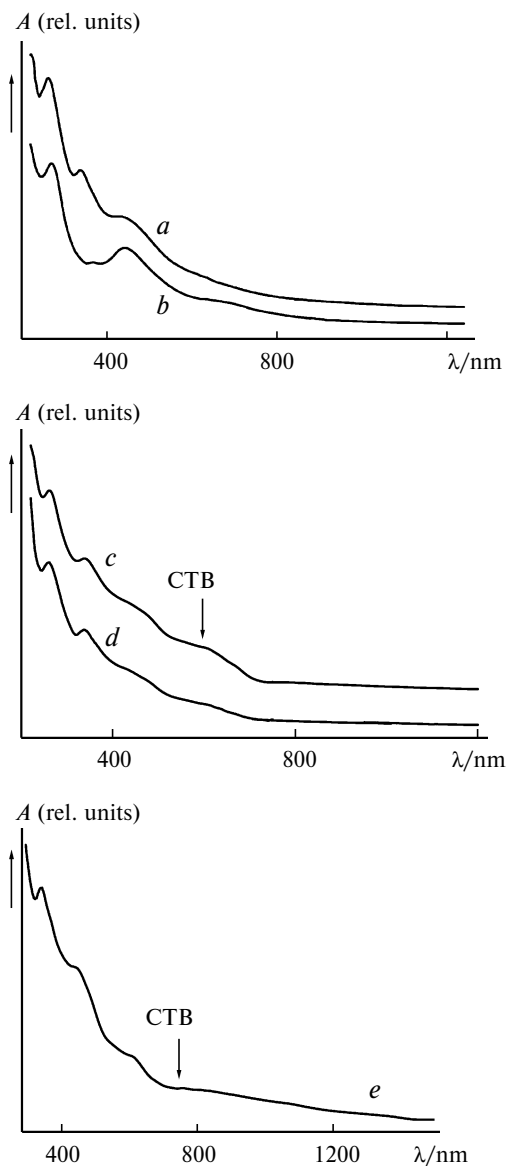


Fig. 9. Absorption spectra of the complexes and donors in the UV-Vis and near-IR regions: $\{\text{Cu}^{II}(\text{Et}_2\text{dtc})_2\}_2 \cdot \text{C}_{60}$ (**2**) (*a*); starting $\text{Cu}^{II}(\text{Et}_2\text{dtc})_2$ (*b*); $\{\text{Cd}(\text{Et}_2\text{dtc})_2\}_2 \cdot \text{C}_{60}$ (**3**) (*c*); $\text{Zn}(\text{Et}_2\text{dtc})_2 \cdot \text{C}_{60} \cdot (\text{C}_6\text{H}_5\text{Cl})_{0.5} \cdot (\text{C}_6\text{H}_6)_{0.5}$ (**16**) (*d*); $[\{\text{Fe}^{II}(\text{Et}_2\text{dtc})_2\}_2 \cdot \text{DABCO}] \cdot \text{C}_{60} \cdot (\text{DABCO})_2$ (**11**) (*e*).

C₆₀ layers. Actually, the band at 470 nm is observed in the spectra of these complexes. In the spectra of complexes **3** and **11**, additional broad absorption bands are observed in the visible and near-IR regions at 610 and 760 nm, respectively (see Fig. 9, *c*, *e*). These bands are absent in the spectra of the starting fullerenes and dithiocarbamates. They are associated with charge transfer from HOMO of dithiocarbamate to LUMO of fullerene due to the overlapping of these π orbitals in the complexes. Analogously, the spectra of **4–6**, **9**, **10**, **12**, and **14** also show broad charge transfer bands in the visible region (600–800 nm).

In complex **5**, the π – π interaction with C_{60} is absent and no charge transfer bands are observed in its spectrum (see Fig. 10, *d*) (intensity of the absorption band at 600 nm is equal to that in the spectrum of the starting fullerene C_{60} and, consequently, this band can be assigned to symmetry forbidden transitions in C_{60}). The absorption bands characteristic of the $C_{60}^{\cdot-}$ radical anions at 946–960 and 1070–1080 nm are absent in the spectra of complexes **1–16**, which is indicative of the molecular character of these complexes and is consistent with the ESR data.

5. Photoconductivity of complexes

Crystals of complexes **2**, **3**, **9**, and **14** exhibit low dark conductivity, $\sigma \approx 10^{-10}$ – 10^{-11} S cm $^{-1}$. The photoexcitation of the crystals with visible light from a halogen lamp in the 260–850 nm region with a power of 150 W and a light flux of 10^{12} – 10^{14} photon cm $^{-2}$ s $^{-1}$ leads to an increase in the photocurrent by two–three orders of magnitude. These values remain constant over a long period of time (10^4 s) and are completely reproducible. This is evidence of the absence of nonequilibrium processes associated with photostimulated chemical or structural transformations of materials.

The photoconductivity spectra of complexes **2** and **3** are presented in Fig. 10. The photoconductivity has

maxima at 470 nm for **2** and \sim 660 nm for **3**. The visible light irradiation of the complexes in the 260–850 nm region can give rise to both the photoexcitation of the donor or fullerene molecule and the charge transfer between the adjacent fullerene molecules or, alternatively, from the donor molecule to the fullerene molecule. These processes are induced by excitation at different wavelengths. A comparison of the photoconductivity spectra with the absorption spectra of the complexes suggests the mechanisms of generation of free charge carriers. For example, the position of the maximum of photoconductivity in complex **2** is close to that of the absorption band of $Cu(Et_2dtc)_2$ (437 nm) and the absorption band associated with the charge transfer between the C_{60} molecules (maximum at 470 nm). Consequently, both these processes can contribute to the photoconductivity. In the spectrum of complex **3**, the position of the maximum of photoconductivity is close to that of the band associated with the charge transfer from $\{Cd(Et_2dtc)_2\}_2$ to C_{60} (610 nm), whereas the contribution of the charge transfer between C_{60} (470 nm) is insignificant (see Fig. 10, *b*). Therefore, in spite of the similar crystal structures, the mechanisms of generation of free charge carriers in complexes **2** and **3** are different.

The maxima in the photoconductivity spectra of complexes **9** and **14** (see Fig. 10, *c, d*) are observed at

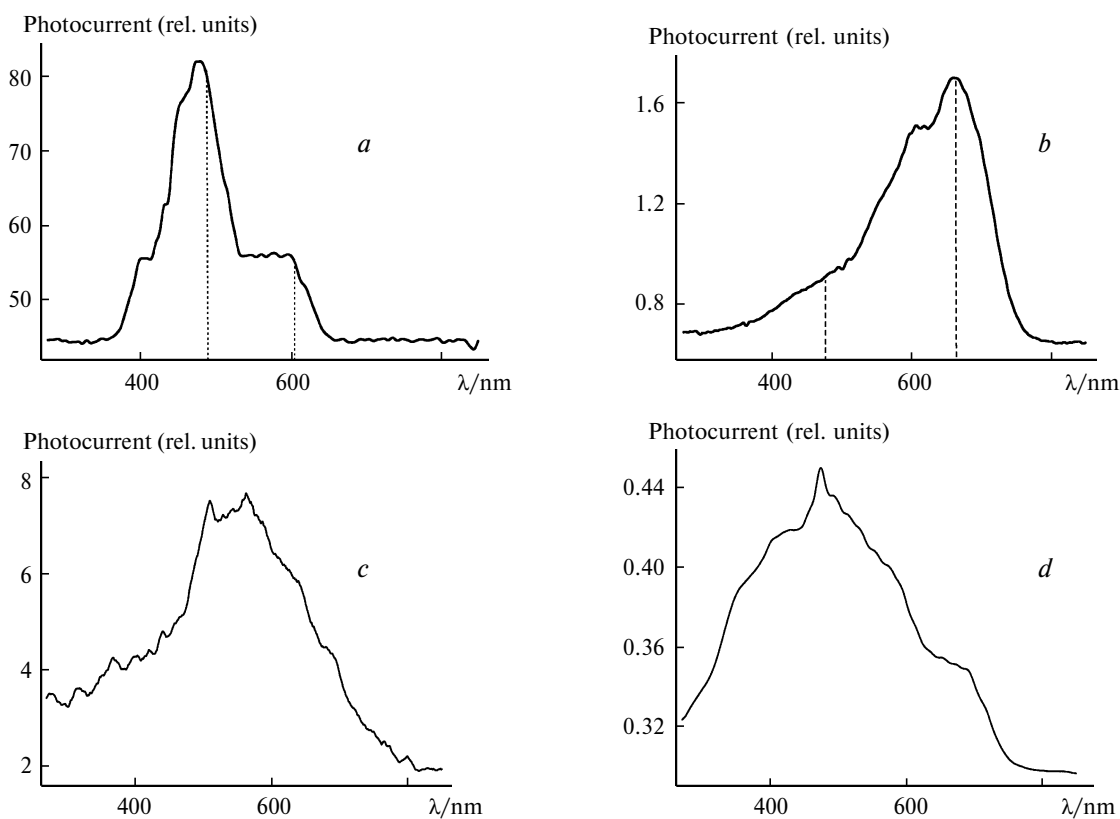


Fig. 10. Photoconductivity spectra of the complexes in the 260–850 nm region: $\{Cu^{II}(Et_2dtc)_2\}_2 \cdot C_{60}$ (**2**) (*a*); $\{Cd(Et_2dtc)_2\}_2 \cdot C_{60}$ (**3**) (*b*); $[\{Zn(Et_2dtc)_2\}_2 \cdot DABCO] \cdot C_{60} \cdot (DABCO)_2$ (**9**) (*c*); $[\{Zn(Et_2dtc)_2\} \cdot HMTA]_2 \cdot C_{60} \cdot C_6H_5Cl$ (**14**) (*d*).

500–600 nm (**9**) and 474 and 685 nm (**14**). In the case of **9**, the charge transfer from $\{\text{Zn}(\text{Et}_2\text{dtc})_2\}_2 \cdot \text{DABCO}$ to C_{60} makes the major contribution to the generation of free charge carriers, whereas both the charge transfer between the C_{60} molecules (474 nm) and the charge transfer from $\{\text{Zn}(\text{Et}_2\text{dtc})_2\} \cdot \text{HMTA}$ to C_{60} (685 nm) can make the contribution in the case of **14**.

* * *

To summarize, we synthesized a series of C_{60} and C_{70} complexes with metal(II) dithiocarbamates $\{\text{M}^{\text{II}}(\text{R}_2\text{dtc})_2\} \cdot \text{C}_{60}$, $\{\text{M}^{\text{II}}(\text{R}_2\text{dtc})_2\} \cdot \text{C}_{70}$ and metal dithiocarbamates coordinated to nitrogen-containing ligands, $\{\text{M}^{\text{II}}(\text{R}_2\text{dtc})_2\}_x \cdot \text{L} \cdot \text{C}_{60}$ (**1–16**). The cocrystallization of most of dithiocarbamates with fullerenes affords the dinuclear structures $\{\text{M}^{\text{II}}(\text{Et}_2\text{dtc})_2\}_2$, which are compatible with the spherical shape of C_{60} molecules. These complexes are characterized by the efficient π – π interaction between the fragments of dithiocarbamates and C_{60} . Some dithiocarbamates ($\text{M} = \text{Cd}, \text{Mn}, \text{or Fe}$) cause the almost complete precipitation of fullerenes C_{60} and C_{70} as complexes from different solvents. The shape of coordinated dithiocarbamates $\{\text{M}^{\text{II}}(\text{Et}_2\text{dtc})_2\}_x \cdot \text{L}$ ($x = 1$ and 2 ; L is HMTA or DABCO) is also consistent well with the spherical shape of C_{60} . The dihedral angle between the MS_2CN planes in dithiocarbamates optimum for π – π interactions with C_{60} is in the range of 144 – 149° (complexes **3**, **4**, and **10–12**). An increase or decrease in the dihedral angles in dithiocarbamates leads to a weakening of π – π interactions (complexes **1**, **2**, **13**, and **15**). The efficient π – π interaction in the complexes leads to the ordering of the C_{60} molecules and gives rise to charge transfer bands from metal dithiocarbamates to C_{60} .

Most of fullerene complexes with dithiocarbamates have layered structures. The arrangement of the fullerene molecules in the layers varies from hexagonal to square. The layers can be either close-packed or contain isolated fullerene molecules. The packing of fullerenes in the layers is determined by the metal atoms in dithiocarbamates and the length of their alkyl substituents. In the C_{60} complexes with $\text{Zn}(\text{Et}_2\text{dtc})_2$ and $\{\text{Hg}(\text{Pr}^n_2\text{dtc})_2\}_2 \cdot \text{DMP}$, the C_{60} molecules form a three-dimensional close packing.

It is known that Mn^{II} and Fe^{II} dithiocarbamates are rather strong donors. However, the charge transfer is absent in C_{60} complexes with these dithiocarbamates. The optical spectra confirm the neutral ground state of complexes **1–16**. Changes in the ESR spectra of dithiocarbamates upon the complex formation with fullerenes are associated primarily with changes in the local environment of the metal atoms. For example, the formation of complexes **1** and **2** is accompanied by a weak coordination of Cu^{II} atoms to the C_{60} molecule and the flattening of the central $\text{Cu}(\text{S}_2\text{CN})_2$ fragment. Considerable changes in the ESR spectrum of $\text{Mn}(\text{Et}_2\text{dtc})_2$ upon the formation

of complex **6** are most likely caused by the transformation of the polynuclear structure of the starting Mn^{II} dithiocarbamate into the dinuclear structure $\{\text{Mn}(\text{Et}_2\text{dtc})_2\}_2$ in complex **6**. The dinuclear structure $\{\text{Fe}^{\text{II}}(\text{Et}_2\text{dtc})_2\}_2$ is characterized by the presence of the short axial $\text{M}—\text{S}$ bond providing the magnetic coupling. This is, apparently, responsible for the strong antiferromagnetic interactions between the metal atoms in complexes **5** and **6**. The presence of the long axial $\text{M}—\text{S}$ bond in Cu^{II} dithiocarbamates (**1** and **2**) leads only to weak antiferromagnetic interactions. In the coordinated $\{\text{M}^{\text{II}}(\text{Et}_2\text{dtc})_2\}_2 \cdot \text{DABCO}$ dinuclear moieties, the distance between the metal atoms is longer than that in the dinuclear structures $\{\text{M}^{\text{II}}(\text{Et}_2\text{dtc})_2\}_2$. This leads to a weakening of the magnetic coupling between the metal atoms in the complexes and changes from antiferromagnetic to ferromagnetic interactions of spins.

The complexes exhibit low dark conductivity. The visible light irradiation of crystals of the complexes leads to an increase in the photocurrent by two–three orders of magnitude. A comparison of the photoconductivity spectra with the absorption spectra of the complexes allows the conclusion that the photoexcitation of $\text{Cu}^{\text{II}}(\text{Et}_2\text{dtc})_2$ makes the major contribution to the photogeneration of charge carriers in complex **2**, whereas the major contribution in complex **3** is made by the charge transfer from $\text{Cd}(\text{Et}_2\text{dtc})_2$ to C_{60} . The difference in the mechanism of photoconductivity in the complexes is associated with the light absorption at different wavelengths, because $\text{Cu}^{\text{II}}(\text{Et}_2\text{dtc})_2$ exhibits strong absorption in the visible region (442 nm), whereas $\text{Cd}(\text{Et}_2\text{dtc})_2$ does not show absorption in this region. It should be noted that $\text{Cd}(\text{Et}_2\text{dtc})_2$ is characterized by the more efficient π – π interaction with C_{60} compared to $\text{Cu}^{\text{II}}(\text{Et}_2\text{dtc})_2$, resulting in the appearance of the charge transfer band in the spectrum of **3** at 610 nm. As in the case of complex **3**, the charge transfer from metal dithiocarbamate to the C_{60} molecule makes the major contribution to the photoconductivity of complexes with coordinated dithiocarbamates. Earlier, it has been demonstrated that if a donor exhibits intense absorption in the visible region (for example, tetrabenzoz(1,2-bis[4*H*-thiopyran-4-ylidene]ethane) (Bz_4BTPE), the photoconductivity in the complex with C_{60} is determined primarily by the photoexcitation of the donor.⁵⁶ If the spectrum shows an intense charge transfer band (for example, the spectrum of $\text{TBPDA} \cdot (\text{C}_{60})_2$, where TBPDA is tetrabenzyl-*p*-phenylenediamine), the photoconductivity is determined primarily by the charge transfer from the donor to the C_{60} molecule.⁵⁷ The charge transfer between the fullerene molecules, which is observed in crystals⁵⁸ and films⁵⁴ of C_{60} and in the C_{60} complexes with Bz_4BTPE ⁵⁶ and TBPDA,⁵⁷ also contributes to the photoconductivity. The appearance of the photoconductivity in the complexes under consideration is associated with the steric compatibility between the

shapes of the donors and C₆₀ and their layered packing, which provides the efficient charge phototransfer and allows the photoinduced charge carriers to move in the crystals along the layers.

Experimental

Sodium diethyldithiocarbamate Na(Et₂dtc)·3H₂O, diazabicyclooctane (DABCO), *N,N'*-dimethylpiperazine (DMP), hexamethylenetetramine (HMTA) (Aldrich), Zn(Buⁿ₂dtc)₂ (Wako), fullerene C₆₀ of 99.98% purity, and fullerene C₇₀ of 99.90% purity were used. Sodium di(isopropyl)dithiocarbamate, Na(Prⁱ₂dtc), and sodium di(*n*-propyl)dithiocarbamate, Na(Prⁿ₂dtc), were synthesized and purified according to a procedure described earlier.²¹ Anhydrous sodium diethyldithiocarbamate, Na(Et₂dtc), was prepared by recrystallization from an acetonitrile–benzene mixture. Dithiocarbamates Fe^{II}(Et₂dtc)₂ and Mn^{II}(Et₂dtc)₂ and their complexes with fullerenes are sensitive to oxygen and were synthesized in an inert atmosphere box with an oxygen and water content lower than 1 ppm. After distillation, all solvents were purified from oxygen by three freezing–evacuation–filling with argon–thawing cycles. Metal dithiocarbamates were synthesized by mixing the corresponding anhydrous metal salt (~0.7 mmol) and two molar equivalents of Na(R₂dtc) in acetonitrile (10 mL) for 4 h. Dithiocarbamates M(R₂dtc)₂ precipitated from acetonitrile together with the corresponding sodium salts. The precipitates were filtered off, washed with acetonitrile, and dissolved in chlorobenzene or toluene. Sodium salts were separated by filtration. Pure metal dithiocarbamates were isolated by removing the solvent on a rotary evaporator. Dichlorobenzene (C₆H₄Cl₂), chlorobenzene (C₆H₅Cl), and acetonitrile were purified by distillation over CaH₂. Hexane was distilled over Na/benzophenone. Crystals of complexes **5**, **6**, **11**, and **12** are sensitive to oxygen and they were stored in an inert atmosphere box. To perform ESR and magnetic measurements, samples were sealed in 2-mL quartz tubes under helium; KBr pellets for UR, UV-Vis, and near-IR spectroscopy were prepared in an inert atmosphere box.

Table 5. Composition and elemental analysis data for complexes **5–9**

| Complex | Found (%) | | | | Calculated (%) | |
|----------|-----------|------|------|------|----------------|-------|
| | C | H | Cl | N | M | S |
| 5 | 66.02* | 2.64 | <0.4 | 3.87 | | |
| | 67.44 | 2.80 | — | 3.93 | 7.86 | 17.97 |
| 6 | 68.88* | 2.59 | — | 3.69 | | |
| | 70.05 | 2.98 | — | 3.63 | 7.13 | 16.60 |
| 7 | 86.74 | 1.48 | — | 1.44 | | |
| | 86.67 | 1.51 | — | 1.51 | 3.42 | 6.89 |
| 8 | 87.80 | 1.95 | 1.14 | 1.20 | | |
| | 87.58 | 1.72 | 1.49 | 1.17 | 2.68 | 5.36 |
| 9 | 66.12 | 3.84 | — | 7.97 | | |
| | 65.95 | 4.29 | — | 7.91 | 7.39 | 14.46 |

* The carbon content is lower than the calculated values because of sensitivity of these complexes to oxygen.

Synthesis of complexes. The compositions of complexes **5–9** were determined by elemental analysis (Table 5). The compositions of complexes **1–4** and **10–16** were determined by X-ray diffraction. Several crystals, which were prepared in the same synthesis and tested by X-ray diffraction, have identical unit cell parameters.

Crystals of complexes **1**, **2**, **7**, **8**, and **16** were grown by evaporation of a solution containing C₆₀ (25 mg, 0.0347 mmol) and a twofold molar excess of metal dithiocarbamate in PhCl (15 mL) for one week. The crystals were washed with acetone and dried in air (50–80% yields). The crystals were dark-brown or black and were rhombus-shaped (**1**), hexagonal plate-like (**2**), thin needle-like (**7**, **8**), or prismatic (**16**).

In the presence of dithiocarbamates Cd(Et₂dtc)₂, Mn(Et₂dtc)₂, and Fe(Et₂dtc)₂, fullerenes C₆₀ and C₇₀ precipitated as the corresponding complexes from various solvents (C₆H₆, PhCl, and C₆H₄Cl₂) in virtually quantitative yields. Because of this, the crystals of complexes **3**, **5**, and **6** were grown by the diffusion method. A benzene solution of fullerene (20 mL, 0.0238 mmol) was layered onto a solution (20 mL) of Cd(Et₂dtc)₂ in CHCl₃ (**3**) or onto a solution (20 mL) of Mn(Et₂dtc)₂ or Fe(Et₂dtc)₂ in C₆H₄Cl₂ (**5** and **6**). A twofold molar excess of dithiocarbamates was used. The crystals of the complexes formed on the walls of diffusion tubes after storage for approximately one month. The solvent was decanted from the crystals and the crystals were washed with hexane (50–60% yields). Dark-brown crystals were rhombus-shaped (**3**) or elongated parallelepiped-shaped (**5** and **6**).

Crystals of complexes **4** and **9–13** were grown by the diffusion method. Dithiocarbamates M(Et₂dtc)₂ (**4**, **9**, **12**) (42–48 mg, 0.105 mmol) or Cd(Prⁱ₂dtc)₂ (**13**) (53 mg, 0.105 mmol), excess DABCO (100 mg, 0.9 mmol), and C₆₀ (25 mg, 0.035 mmol) were dissolved in C₆H₄Cl₂ (12 mL) at 60 °C for 4 h. The solution was cooled and filtered into a 45-mL diffusion tube. Then hexane (30 mL) was layered onto the reaction solution. The diffusion time was two months. The crystals formed on the walls of the tube in the hexane portion of the solution. Complexes **9–13** contain dinuclear dithiocarbamates coordinated to DABCO; however, according to the X-ray diffraction study, DABCO is not involved in complex **4** ({Hg(Et₂dtc)₂})₂·C₆₀.

Crystals of [{Hg(Prⁿ₂dtc)₂}]₂·DMP·(C₆₀)₅·(C₆H₅Cl)₄ (**15**) were grown by concentrating a chlorobenzene solution (15 mL) containing Hg(Prⁿ₂dtc)₂ (58 mg, 0.105 mmol), C₆₀ (25 mg, 0.035 mmol), and excess DMP (1 mL). After evaporation of the solvent for 1 week, crystals of **15** were grown as black prisms with dimensions up to 2×1×0.5 mm. The crystals were filtered off and washed with acetone (75% yield).

Crystals of [{Zn(Et₂dtc)₂}]₂·HMTA]·C₆₀·C₆H₅Cl (**14**) were grown by concentrating a 15 : 1 C₆H₅Cl/C₆H₅CN solution (16 mL) containing Zn(Et₂dtc)₂ (38 mg, 0.105 mmol), C₆₀ (25 mg, 0.035 mmol), and excess HMTA (40 mg, 0.28 mmol). Once the solution was concentrated to 1–2 mL, the solvent was decanted, and the crystals were washed with acetone. Black prismatic crystals were obtained in 80% yield.

The UV-Vis and near-IR spectra were recorded on a Shimadzu-3100 instrument in the 240–2600 nm region in KBr pellets. The IR spectra were measured on a Perkin-Elmer 1000 instrument in the 400–7800 cm⁻¹ region in KBr pellets. The magnetic properties of complexes **1**, **2**, **5**, **6**, **11**, and **12** were studied on a Quantum Design MPMS-XL SQUID

Table 6. Principal crystallographic data for complexes **4** and **10–12**

| Parameter | 4 | 10 | 11 | 12 |
|---|---|--|--|--|
| Formula | C ₈₈ H ₄₀ Hg ₂ N ₄ S ₈ | C ₉₈ H ₇₆ Cd ₂ N ₁₀ S ₈ | C ₉₈ H ₇₆ Mn ₂ N ₁₀ S ₈ | C ₉₈ H ₇₆ Fe ₂ N ₁₀ S ₈ |
| M | 1714.82 | 1870.94 | 1760.05 | 1757.84 |
| Crystal system | Monoclinic | Orthorhombic | Orthorhombic | Orthorhombic |
| Space group | <i>P2₁/n</i> | <i>Pbam</i> | <i>Pbam</i> | <i>Pbam</i> |
| <i>a</i> /Å | 16.1521(5) | 10.4576(3) | 10.44310(4) | 10.3490(4) |
| <i>b</i> /Å | 16.9573(4) | 17.0583(5) | 17.0608(6) | 16.9698(7) |
| <i>c</i> /Å | 10.5560(3) | 20.9776(5) | 20.9215(7) | 20.8387(9) |
| α /deg | 90 | 90 | 90 | 90 |
| β /deg | 99.7330(10) | 90 | 90 | 90 |
| γ /deg | 90 | 90 | 90 | 90 |
| <i>V</i> /Å ³ | 2849.63(14) | 3742.2(2) | 3726.8(2) | 3659.7(3) |
| <i>Z</i> | 2 | 2 | 2 | 2 |
| <i>d</i> _{calc} /g cm ⁻³ | 1.999 | 1.660 | 1.568 | 1.595 |
| μ /mm ⁻¹ | 5.733 | 0.854 | 0.626 | 0.689 |
| <i>T</i> _{exp} /K | 100(2) | 90(1) | 100(2) | 90(1) |
| 2 θ _{max} /deg | 56.56 | 77.46 | 56.56 | 68.65 |
| Number of reflections | 23241 | 165581 | 24899 | 73217 |
| Number of independent reflections | 6956 | 10623 | 4708 | 7539 |
| Number of parameters /restraints | 429/0 | 292/0 | 305/3 | 292/0 |
| Number of reflections with <i>I</i> > 2 σ (<i>I</i>) | 6294 | 9580 | 4415 | 6663 |
| <i>R</i> Factor (<i>I</i> > 2 σ (<i>I</i>)) | 0.0218 | 0.0237 | 0.0364 | 0.0342 |
| <i>wR</i> | 0.0711 | 0.0681 | 0.1130 | 0.1565 |
| CCDC | 638243 | 614489 | 638245 | 614490 |

Table 7. Principal crystallographic data for complexes **13–15**

| Parameter | 13 | 14 | 15 |
|---|--|--|--|
| Formula | C ₁₀₀ H _{80.80} Cd ₂ Cl _{0.24} N ₆ S ₈ | C ₉₈ H ₆₉ ClN ₁₂ S ₈ Zn ₂ | C ₃₅₈ H ₉₀ Cl ₄ Hg ₂ N ₆ S ₈ |
| M | 1856.29 | 1837.32 | 5273.82 |
| Crystal system | Orthorhombic | Triclinic | Monoclinic |
| Space group | <i>Ibam</i> | <i>P</i> $\bar{1}$ | <i>P2₁/n</i> |
| <i>a</i> /Å | 11.7155(3) | 10.3921(4) | 16.9422(11) |
| <i>b</i> /Å | 16.5374(4) | 16.9217(6) | 20.1412(13) |
| <i>c</i> /Å | 42.0900(8) | 22.3916(8) | 29.786(2) |
| α /deg | 90 | 84.1470(10) | 90 |
| β /deg | 90 | 76.6500(10) | 94.9170(10) |
| γ /deg | 90 | 89.8850(10) | 90 |
| <i>V</i> /Å ³ | 8154.7(3) | 3810.3(2) | 10126.6(11) |
| <i>Z</i> | 4 | 2 | 2 |
| <i>d</i> _{calc} /g cm ⁻³ | 1.512 | 1.601 | 1.730 |
| μ /mm ⁻¹ | 0.790 | 0.948 | 1.731 |
| <i>T</i> _{exp} /K | 100(2) | 95(2) | 100(2) |
| 2 θ _{max} /deg | 54.96 | 54.2 | 56.5 |
| Number of reflections | 30288 | 24119 | 52049 |
| Number of independent reflections | 4704 | 16328 | 24480 |
| Number of parameters /restraints | 442/373 | 1153/115 | 1776/1825 |
| Number of reflections with <i>I</i> > 2 σ (<i>I</i>) | 4126 | 14634 | 21358 |
| <i>R</i> Factor (<i>I</i> > 2 σ (<i>I</i>)) | 0.0252 | 0.0376 | 0.0561 |
| <i>wR</i> | 0.0618 | 0.0885 | 0.1501 |
| CCDC | 638242 | 638246 | 638244 |

magnetometer in the temperature range of 1.9–300 K in the magnetic field of 100 mT. The contribution of the sample holder and the diamagnetic contribution (χ_0) were subtracted from the experimental data. The parameters Θ and χ_0 were calculated by fitting the experimental data according to the equation

$$\chi_M = C/(T - \Theta) + \chi_0.$$

For complexes **1** and **2**, the experimental data in the temperature range of 10–300 K were used; for **11** and **12**, in the range of 50–300 K; for **6**, in the range of 150–300 K; for **5**, in the range of 200–300 K. The ESR spectra were recorded at 295 and 4 K on a JEOL JES-TE 200 instrument. The photoconductivity spectra were measured at 293 K using light from a xenon lamp passed through a monochromator. To study the influence of the magnetic field on the photoconductivity, the complexes were irradiated with white light from a halogen lamp with an intensity of 10^{12} – 10^{14} photons $\text{cm}^{-2} \text{s}^{-1}$. A single crystal in a quartz tube was placed in a cell of a standard RadioPan SE/X 2547 spectrometer. The voltage at silver contacts pasted to one surface of the crystal was 10–50 V.

X-ray diffraction study. The X-ray diffraction data sets for complexes **4** and **10–15** were collected on a Bruker Nonius X8 diffractometer equipped with a CCD detector (Mo-K α radiation, $l = 0.71073 \text{ \AA}$) and an Oxford Cryosystems cryostat (ϕ - and ω -scanning technique with a frame width of 0.3° ; the exposure time per frame was 30 s). The data were integrated, scaled, and merged using the Bruker AXS software.⁵⁹ Absorption corrections were applied using the SADABS program.⁶⁰ The structures were solved by direct methods with the use of the SHELX 97 program package⁶¹ and refined by the least-squares method based on F^2 . The nonhydrogen atoms were refined anisotropically. The hydrogen atoms were positioned geometrically. Principal crystallographic data, including the deposition numbers at the Cambridge Crystallographic Data Centre, for complexes **4** and **10–15** are given in Tables 6 and 7. The crystallographic data for complexes **1** (CCDC 288292), **2** (CCDC 260289), **3** (CCDC 286144), and **16** (CCDC 288291) have been published earlier.^{31,32}

The C₆₀ and metal dithiocarbamate molecules are ordered in almost all complexes. In complex **13**, the C₆₀ molecules are disordered between two orientations with occupancies of 0.75/0.25. One of three crystallographically independent C₆₀ molecules in **15** is randomly disordered. In complexes **10–13**, the DABCO molecule is randomly disordered between two orientations related by the rotation by 60° about the axis passing through two nitrogen atoms. In complex **14**, the molecule of the PhCl solvent is disordered between four orientations. In complex **4**, the position of the solvent molecule is occupied by disordered hexane (84%) and C₆H₄Cl₂ (16%) molecules. In complex **15**, PhCl molecules occupy two positions. In one position, the PhCl molecule is disordered between two orientations; in another position, between three orientations.

This study was financially supported by the Russian Foundation for Basic Research (Project Nos 06-03-32824, 06-03-91361, and 06-02-96323), the INTAS (Young Scientist Fellowship Grant YSF 05-109-4653), the Council on Grants of the President of the Russian Federation (Program for State Support of Leading Scientific Schools of the Russian Federation and of Young Scientists, Grant

MK-932.2007.2), and the Russian Science Support Foundation.

References

1. D. V. Konarev and R. N. Lyubovskaya, *Usp. Khim.*, 1999, **68**, 23 [*Russ. Chem. Rev.*, 1999, **68**, 19 (Engl. Transl.)].
2. D. M. Guldi, *Chem. Soc. Rev.*, 2002, **31**, 22.
3. B. Gotschy, *Fullerene Sci. Technol.*, 1996, **4**, 677.
4. D. V. Konarev, Yu. V. Zubavichus, E. F. Valeev, Yu. L. Slovokhotov, Yu. M. Shul'ga, and R. N. Lyubovskaya, *Synth. Met.*, 1999, **103**, 2364.
5. A. L. Litvinov, D. V. Konarev, A. Yu. Kovalevsky, I. S. Neretin, Yu. L. Slovokhotov, P. Coppens, and R. N. Lyubovskaya, *CrystEngComm.*, 2002, **4**, 618.
6. G. A. Domrachev, Yu. A. Shevelev, V. K. Cherkasov, G. F. Fukin, G. V. Markin, and A. I. Kirilov, *Izv. Akad. Nauk, Ser. Khim.*, 2006, 220 [*Russ. Chem. Bull., Int. Ed.*, 2006, **55**, 225].
7. A. Izuoka, T. Tachikawa, T. Sugawara, Y. Suzuki, M. Konno, Y. Saito, and H. Shinohara, *J. Chem. Soc., Chem. Commun.*, 1992, 1472.
8. D. V. Konarev, R. N. Lyubovskaya, N. V. Drichko, E. I. Yudanov, Yu. M. Shul'ga, A. L. Litvinov, V. N. Semkin, and B. P. Tarasov, *J. Mat. Chem.*, 2000, 803.
9. S. V. Konovalikhin, O. N. D'yachenko, G. V. Shilov, N. G. Spitsina, K. V. Van, and E. B. Yagubskii, *Izv. Akad. Nauk, Ser. Khim.*, 1997, 1480 [*Russ. Chem. Bull.*, 1997, **46**, 1415 (Engl. Transl.)].
10. V. A. Nadtochenko, V. V. Gritsenko, O. N. D'yachenko, G. V. Shilov, and A. P. Moravskii, *Izv. Akad. Nauk, Ser. Khim.*, 1996, 1285 [*Russ. Chem. Bull.*, 1996, **45**, 1224 (Engl. Transl.)].
11. D. V. Konarev, A. Yu. Kovalevsky, A. L. Litvinov, N. V. Drichko, B. P. Tarasov, P. Coppens, and R. N. Lyubovskaya, *J. Solid State Chem.*, 2002, **168**, 474.
12. E. I. Yudanov, D. V. Konarev, R. N. Lyubovskaya, and L. L. Gumanov, *Izv. Akad. Nauk, Ser. Khim., Izv. Akad. Nauk, Ser. Khim.*, 1999, 722 [*Russ. Chem. Bull.*, 1999, **48**, 718 (Engl. Transl.)].
13. M. M. Olmstead, D. A. Costa, K. Maitra, B. C. Noll, S. L. Phillips, P. M. Van Calcar, and A. L. Balch, *J. Am. Chem. Soc.*, 1999, **121**, 7090.
14. D. V. Konarev, I. S. Neretin, Yu. L. Slovokhotov, E. I. Yudanov, N. V. Drichko, Yu. M. Shul'ga, B. P. Tarasov, L. L. Gumanov, A. S. Batsanov, J. A. K. Howard, and R. N. Lyubovskaya, *Chem. Eur. J.*, 2001, **7**, 2605.
15. A. L. Balch and M. M. Olmstead, *Chem. Rev.*, 1998, **98**, 2123.
16. D. V. Konarev, I. S. Neretin, A. L. Litvinov, N. V. Drichko, Yu. L. Slovokhotov, R. N. Lyubovskaya, J. A. K. Howard, and D. S. Yufit, *Cryst. Growth Des.*, 2004, **4**, 643.
17. A. L. Litvinov, D. V. Konarev, A. Yu. Kovalevsky, P. Coppen, and R. N. Lyubovskaya, *Cryst. Growth Des.*, 2005, **5**, 1807.
18. D. V. Konarev, S. S. Khasanov, A. Otsuka, G. Saito, and R. N. Lyubovskaya, *Chem. Eur. J.*, 2006, **12**, 5225.
19. D. V. Konarev, S. S. Khasanov, A. Otsuka, G. Saito, and R. N. Lyubovskaya, *J. Am. Chem. Soc.*, 2006, **128**, 9292.
20. D. V. Konarev, S. S. Khasanov, G. Saito, A. Otsuka, and R. N. Lyubovskaya, *Inorg. Chem.*, 2007, **46**, 7601.

21. F. Jian, Z. Wang, Z. Bai, X. You, H.-K. Fun, K. Chinnakali, and I. A. Razak, *Polyhedron*, 1999, **18**, 3401.
22. A. Domenicano, L. Torelli, A. Vaciago, and L. Zambonelli, *J. Chem. Soc. A*, 1968, 1351.
23. F. Jian, Z. Wang, Z. Bai, X. You, H.-K. Fun, and K. Chinnakali, *J. Chem. Cryst.*, 1999, **29**, 227.
24. A. Ieperuma and R. D. Feltham, *Inorg. Chem.*, 1975, **14**, 3042.
25. M. Bonamico, G. Mazzone, A. Vaciago, and L. Zambonelli, *Acta Crystallogr.*, 1965, **19**, 898.
26. N. Sreehari, B. Varghese, and P. T. Manoharan, *Inorg. Chem.*, 1990, **29**, 4011.
27. H. L. M. Van Gaal and J. G. M. Van der Linden, *Coord. Chem. Rev.*, 1982, **47**, 41.
28. H. H. Wickman, A. M. Trozzolo, H. J. Williams, G. W. Hull, and F. R. Merritt, *Phys. Rev.*, 1967, **155**, 563.
29. M. Decoster, F. Conan, J. E. Guerchais, Y. Le Mest, J. Sala Pala, J. C. Jeffery, E. Faulques, A. Leblanc, and P. Molinié, *Polyhedron*, 1995, **14**, 1741.
30. F. Conan, J. Sala Pala, M.-T. Garland, and R. Baggio, *Inorg. Chem. Acta*, 1998, **278**, 108.
31. D. V. Konarev, A. Yu. Kovalevsky, D. V. Lopatin, V. V. Rodaev, A. V. Umrikhin, E. I. Yudanov, P. Coppens, R. N. Lyubovskaya, and G. Saito, *Dalton Trans.*, 2005, 1821.
32. D. V. Konarev, A. Yu. Kovalevsky, S. S. Khasanov, G. Saito, D. V. Lopatin, A. V. Umrikhin, A. Otsuka, and R. N. Lyubovskaya, *Eur. J. Inorg. Chem.*, 2006, 1881.
33. D. V. Konarev, A. Yu. Kovalevsky, A. Otsuka, G. Saito, and R. N. Lyubovskaya, *Inorg. Chem.*, 2005, **44**, 9547.
34. S.-H. Liu, X.-F. Chem, X.-H. Zhu, C.-Y. Duan, and X.-Z. You, *J. Coord. Chem.*, 2001, **53**, 223.
35. C. S. Lai and E. R. T. Tiekink, *Appl. Organomet. Chem.*, 2003, **17**, 251.
36. L. A. Glinskaya, S. M. Zemskova, R. F. Klevtsova, and S. V. Larionov, *Zh. Strukt. Khim.*, 1996, **37**, 176 [*J. Struct. Chem.*, 1996, **37**, 155 (Engl. Transl.)].
37. A. V. Ivanchenko, S. A. Gromilov, S. M. Zemskova, and I. A. Baidina, *Zh. Strukt. Khim.*, 2000, **41**, 106 [*J. Struct. Chem.*, 2000, **41**, 88 (Engl. Transl.)].
38. D. Zeng, M. J. Hampden-Smith, T. M. Alam, and A. L. Rheingold, *Polyhedron*, 1994, **13**, 2715.
39. P. C. Healy and A. H. White, *J. Chem. Soc., Dalton Trans.*, 1973, 284.
40. M. Ciampolini, C. Mengozzi, and P. Orioli, *J. Chem. Soc., Dalton Trans.*, 1975, 2051.
41. R. S. Rowland and R. Taylor, *J. Phys. Chem.*, 1996, **100**, 7384.
42. H.-B. Bürgi, E. Blanc, D. Schwarzenbach, S. Liu, Y. Lu, M. M. Kappes, and J. A. Ibers, *Angew. Chem., Int. Ed. Engl.*, 1992, **31**, 640.
43. O. Kennard, *CRC Handbook of Chemistry and Physics*, Ed. R. C. Weast, CRC Press, Inc., Boca Raton, Florida, 1987, F105.
44. S. V. Khangulov, A. J. Dessiki, V. V. Barynin, D. E. Ass, and G. C. Dismukes, *Biochemistry*, 1995, **34**, 2015.
45. I. Romero, M.-N. Collomb, A. Deronyier, A. Llobet, E. Perret, J. Pèkaut, L. Le Pare, and J.-M. Latour, *Eur. J. Inorg. Chem.*, 2001, 69.
46. C. A. Reed and R. D. Bolskar, *Chem. Rev.*, 2000, **100**, 1075.
47. D. Dubois, K. M. Kadish, S. Flanagan, R. E. Haufler, L. P. F. Chibante, and L. J. Wilson, *J. Am. Chem. Soc.*, 1991, **113**, 4364.
48. H. Miyasaka, N. Matsumoto, N. Re, E. Gallo, and C. Floriani, *Inorg. Chem.*, 1997, **36**, 670.
49. H. J. Choi, J. J. Solol, and J. R. Long, *Inorg. Chem.*, 2004, **43**, 1606.
50. J. Zhang and A. Lachgar, *J. Am. Chem. Soc.*, 2007, **129**, 250.
51. T. Picher, R. Winkler, and H. Kuzmany, *Phys. Rev. B*, 1994, **49**, 15879.
52. M. S. Dresselhaus, G. Dresselhaus, and P. C. Eklund, *Sci. Fullerenes and Carbon Nanotubes*, Academic Press, San Diego, 1996.
53. M. Ichida, A. Nakamura, H. Shinohara, and Y. Saito, *Chem. Phys. Lett.*, 1998, **289**, 579.
54. S. Kazaoui, N. Minami, Y. Tanabe, H. J. Byrne, A. Eilmes, and P. Petelenz, *Phys. Rev. B*, 1998, **58**, 7689.
55. D. V. Konarev, N. V. Drichko, R. N. Lyubovskaya, Yu. M. Shul'ga, A. L. Litvinov, V. N. Semkin, Yu. A. Dubitsky, and A. Zaopo, *J. Mol. Struct.*, 2000, **526**, 25.
56. D. V. Konarev, D. V. Lopatin, V. V. Rodaev, A. V. Umrikhin, S. S. Khasanov, G. Saito, K. Nakasuji, A. L. Litvinov, and R. N. Lyubovskaya, *J. Phys. Chem. Solids*, 2005, **66**, 711.
57. D. V. Lopatin, V. V. Rodaev, A. V. Umrikhin, D. V. Konarev, A. L. Litvinov, and R. N. Lyubovskaya, *J. Mat. Chem.*, 2005, **15**, 657.
58. Yu. A. Ossipyan, Yu. I. Golovin, D. V. Lopatin, R. B. Morgunov, R. K. Nikolaev, and S. Z. Shmurak, *Phys. Stat. Sol. B*, 2001, **223**, R14.
59. *Bruker Analytical X-ray Systems*, Madison, Wisconsin, USA, 1999.
60. Z. Otwinowski and W. Minor, in *Processing of X-ray Diffraction Data Collection in Oscillation Mode, Methods in Enzymology*, Eds C. W. Carter and R. M. Sweet, Academic Press, 1997, 276.
61. G. M. Sheldrick, *SHELX 97*, University of Göttingen, Germany, 1997.

*Received June 28, 2007;
in revised form September 4, 2007*